CO Oxidation as a Prototypical Reaction for Heterogeneous Processes

Hans-Joachim Freund, Gerard Meijer,* Matthias Scheffler,* Robert Schlögl,* and Martin Wolf**

Keywords:
CO oxidation · heterogeneous catalysis · metal clusters · model systems · surface chemistry

Dedicated to Gerhard Ertl on the occasion of his 75th birthday and to the Fritz Haber Institute, Berlin, on occasion of its 100th anniversary

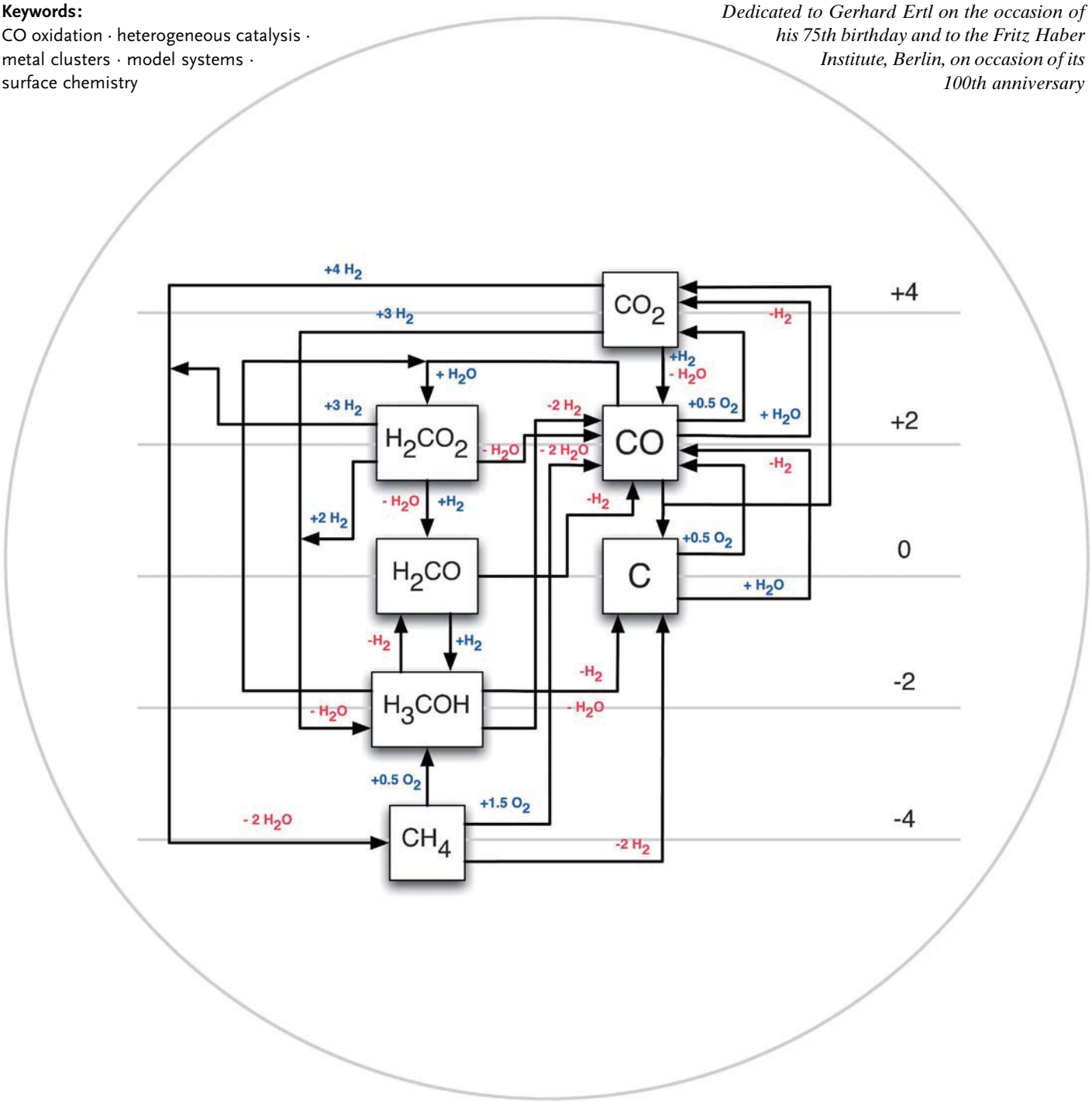

CO oxidation, although seemingly a simple chemical reaction, provides us with a panacea that reveals the richness and beauty of heterogeneous catalysis. The Fritz Haber Institute is a place where a multidisciplinary approach to study the course of such a heterogeneous reaction can be generated in house. Research at the institute is primarily curiosity driven, which is reflected in the five sections comprising this Review. We use an approach based on microscopic concepts to study the interaction of simple molecules with well-defined materials, such as clusters in the gas phase or solid surfaces. This approach often asks for the development of new methods, tools, and materials to prove them, and it is exactly this aspect, both, with respect to experiment and theory, that is a trade mark of our institute.

From the Contents

1. Introduction

Heterogeneous catalysis is the science and technology of transforming molecular structures by using a solid functional material ("the catalyst") to control the energy profile and pathway of a reaction. This control enables the direction and selectivity of the reaction to be determined.

In 1926 H. S. Taylor wrote in his fourth report on the nature of contact catalysis:[1] "*We seem to be forced to the conclusion that we know little or nothing concerning the effect which such aristocracies of atoms exercise on the impinging reactants. … The general problem of activation (of reactants) is of such fundamental importance that every chemist in the world should be keeping it in mind so as to be ready to do his share in the solution*."

Much has changed in our understanding since then, and the "aristocracies of atoms" have been transformed in our understanding into "active sites". The enormous progress in fundamental insights into catalysis is to a great deal due to the understanding of the oxidation of CO as a prototypical reaction for heterogeneous processes. CO oxidation is one of the best-known heterogeneous reactions and can thus be regarded as a benchmark system. However, as will be outlined below, not all facets of this seemingly simple reaction have been explored in sufficient depth to obtain a complete picture of this process.

This Review does not attempt to give an overview of the subject of CO oxidation by presenting a comprehensive account of the literature. It instead attempts to link the evolution of a deeper understanding of one only seemingly simple reaction to the development of our general understanding of heterogeneous processes. The Review further illustrates the close relationship between inventing new experimental and theoretical methods and increased insight into microscopic details of a chemical reaction. A brief account on the evolution of research areas in the field will be followed by an introduction to the chemical relevance of CO oxidation and its role as a prototypical process for elucidating heterogeneous processes. A selection of modern facets of CO oxidation chemistry will then follow, by using selected examples of multidisciplinary research performed at the Fritz Haber Institute in Berlin. This selection will highlight several points raised in the introduction and give an account of the state-of-the-art in regard to the understanding of the reaction over a wide variety of systems and conditions—ranging from isolated molecular clusters over metallic systems of various structures to reactions on complex oxides under high-pressure and high-temperature conditions. It will be shown that some of the systems are of surprising functional complexity even when they appear at first sight to be rather conventional. Their reactivity towards CO and oxygen discloses the complexity that allows us to state that CO oxidation is on its way from a model reaction to a chemical probe for surface properties.

1.1. Research Aspects in CO Oxidation

The toxic character of CO, which is produced in large amounts from the emerging petrochemical industry, prompted early research into strategies to oxidize it at low temperatures with reactive forms of oxygen. Substantial research along these lines was carried out using ozone and various catalysts such as Ag, MnO_2, and PbO during World War I. A review article[2] documents that oxygen atoms alone are poorly reactive and need traces of moisture for effective operation. This is also frequently found today when high reactivity is reported.[3]

The reaction mechanism was studied in great detail much later over noble metals, with unambiguous evidence found for Langmuir–Hinshelwood kinetics.[4] A critical factor is the

[*] Prof. H.-J. Freund, Prof. G. Meijer, Prof. M. Scheffler, Prof. R. Schlögl, Prof. M. Wolf
Fritz Haber Institute of the Max Planck Society
Faradayweg 4–6, 14195 Berlin (Germany)
E-mail: freund@fhi-berlin.mpg.de

availability of sites where both reactants are in proximity, as both reactants can bind strongly to reactive surfaces, thereby forming islands[5] with reactive interfaces and pores in between. The related adsorption and reaction data[4] are cornerstones of quantitative surface science and serve to date as reference points in method development. It is clear today that the respective values are valid not only for extended single crystals but also for oxide-supported nanoparticles when they are prepared under well-defined conditions.[6] The hypothesis that the reaction product CO_2 is inert and does not interfere with the reaction is valid as long as no reducing species are coadsorbed, which neutralize the chemical potential of oxygen. Under these conditions CO_2 is chemisorbed,[7] as is documented by the many reactions involving the hydrogenation of CO_2 in the presence of CO, such as in the synthesis of methanol.

The growing petrochemical industry has resulted in the removal of CO from large gas streams becoming a necessity. Supported noble-metal catalysts were, and still are, used for this purpose. During their application the phenomenon of kinetic oscillations was discovered in critical runaway episodes of the reactors. Several explanations—ranging from a combination of structure sensitivity coupled with restructuring of the catalyst to periodic switching of the catalyst between metallic and oxidation states—were discussed.[8] The use of well-defined single-crystal surfaces and moderate reaction conditions enabled it to be shown by very elegant in situ studies[9] that metal oxide transitions were not involved at the reaction conditions applied but that rather subtle structural dynamic responses[10] ranging from surface reconstructions to subsurface state populations were involved. These findings led to the discovery of the nonlinear dynamic nature of surface reactions[11] and to the evolution of the whole research field[12] of nonlinear dynamics in surface science. In this way, the prototypical character of CO oxidation as a model reaction is uniquely documented.

CO oxidation can also occur when CO is dissolved in water, with OH serving as oxidant. This reaction is of relevance in electrochemistry[13] where fuel cells are inhibited at low processing temperatures by CO poisoning. The reaction can also be used to determine in situ the number of active sites for electrochemical conversions,[14] even when complex polycrystalline supported systems are studied. The desired cleaning of hydrogen streams to remove all traces of CO by selective oxidation to CO_2 is the driving force for one very prominent research field in CO catalysis, namely the application of gold nanoparticles[15] in CO oxidation at or below room temperature. Other catalytic applications of gold nanoparticles are also found in this very active field, but the oxidation of CO is used as an almost universal probe[16] to characterize a wide variety of catalyst systems.

A still highly controversial field of research concerns the nature of the reacting catalyst surface. As oxygen is a reactant, it may occur that not only are adsorbed CO molecules oxidized, but also metallic sites holding the activated oxygen molecules. In the context of unraveling the dynamic response of metal catalysts to CO oxidation under mild conditions, the formation of oxide phases was ruled out. However, when it comes to ambient pressure conditions[17] the situation is less clear, particularly as different authors tend to use different definitions for the term “oxide”, which can be anything between a strongly chemisorbed oxygen adlayer to a separate phase identified by surface crystallography. One review[18] takes a clear position and rules out the role of oxides as high performance catalysts. This is in remarkable contrast to a series of studies on the RuO_2 system, where in similarly unmistakable words[19] the high performance of the oxide phase was stated. The existence of a well-defined surface structure and of high-quality reactivity data prompted a strong evolution of theoretical efforts to predict the reactivity of the RuO_2 system from ab initio calculations. Again the CO

Hans-Joachim Freund (born 1951) studied physics and chemistry at the University of Cologne and received his PhD in 1978. After postdoctoral research at University of Pennsylvania he became associated professor at the University Erlangen-Nürnberg in 1983 and then full professor for physical chemistry at the Ruhr-Universität Bochum in 1987. In 1995 he became a scientific member and director at the Fritz-Haber-Institut der Max-Planck-Gesellschaft in Berlin where he is head of the Department of Chemical Physics. He serves as Adjunct Professor at several universities and he received several national and international awards. His research focuses on the surface science of oxides, nanoparticles, and model catalysts.

Gerard Meijer (born 1962) studied physics at the University of Nijmegen, The Netherlands, and obtained his PhD there in 1988, with spectroscopic studies on small molecules in the gas phase. After postdoctoral research at IBM in San José (characterization of fullerenes) he became full professor in Nijmegen in 1995, where he worked on cavity ring down spectroscopy and launched experimental methods to decelerate and trap neutral polar molecules. As director of the FOM Institute for Plasma Physics in Nieuwegein (2000–2003), he pioneered the use of infrared free electron lasers for the structural characterization of gas-phase clusters and biomolecules. Since 2002 he has been director of the Molecular Physics department at the Fritz-Haber-Institut der Max-Planck-Gesellschaft in Berlin.

Matthias Scheffler (born 1951) studied physics at the Technische Universität Berlin and obtained his PhD in 1978. After working as a staff scientist at the Physikalisch-Technische-Bundesanstalt in Braunschweig, in 1988 he accepted a position as director at the Fritz-Haber-Institut der Max-Planck-Gesellschaft in Berlin, where he has since been head of the Theory Department. His research focuses on understanding fundamental aspects of physical and chemical properties of surfaces, interfaces, clusters, nanostructures, and bulk systems by ab initio electronic-structure theory as well as the development of theoretical methods for calculating total energies and theoretical spectroscopy.

oxidation served as a model system for a methodical development that allowed surface thermodynamics, statistical mechanics, and the related reactivity to predicted from ab inito calculations[20] without using experimental parameters. These results predict a maximum reactivity in a region of the Ru-O phase diagram where a dynamic interplay of surface phases occurs. Remembering the complex control of reactivity over single-crystal elemental metals by the competition for adsorption sites, this finding for an oxide system is not too surprising. The complexity of this system has given rise to a still-ongoing debate.[18,21] Careful experiments on the coupling of surface and subsurface chemistry at elevated chemical potential[22] together with ab initio theoretical studies[20] have elucidated that the different positions in the literature are in fact not controversial, but can instead be considered as elements of a more general picture of a catalyst that responds with complex chemistry to the various chemical potentials applied in different types of experiments. A great deal of the "controversy" resides in the use of the word "oxide". In the interphase between an adsorbate phase of oxygen atoms residing strictly on the outer surface and an oxide characterized by crystallographic methods, several kinetically stabilized states of metal plus oxygen exist that provide enhanced catalytic activity. The various reasons for this enhancement will be discussed in Sections 5 and 6 of.

These examples document both the detailed knowledge and control of the reaction on one side and the still unclear material situation on the other. This lack of understanding arises from fundamental issues of dynamics and reactivity that are observed at elevated chemical potentials. We notice an unexpectedly strong dependence of the stoichiometry and geometry of a catalyst surface on the chemical potential of the reactants (resulting from the composition, temperature, and pressure). It appears that not all the facets of this seemingly simple reaction have been explored over a sufficiently wide range of parameters to obtain the full picture of the dynamic interaction between the reactant and substrate.

Robert Schlögl (born 1954) studied chemistry at the Ludwig-Maximilians-Universität in Munich where he received his PhD in 1982. After postdoctoral stays at Cambridge and Basle he completed his habilitation with Professor Ertl in Berlin. In 1989 he was appointed Professor at Goethe-Universität, Frankfurt, and since 1994 Director of the Department of Inorganic Chemistry at the Fritz-Haber-Institute der Max-Planck-Gesellschaft in Berlin. Key aspects of his research are heterogeneous catalysis with the aim of linking in situ functional analysis with the development of nanochemical concepts. A focus of application is sustainable energy supply. He is currently establishing a Max Planck Institute for Chemical Energy Conversion at the Campus in Mülheim.

Martin Wolf (born 1961) studied physics at the Freie Universität Berlin and received his PhD there in 1991 with Gerhard Ertl. After a postdoctoral period in Austin, Texas, with Mike White, he set up a laboratory for femtosecond surface spectroscopy at the Fritz-Haber-Institute and was also a visiting scientist at IBM Yorktown Heights with Tony Heinz. In 2000 he was appointed full professor for experimental physics at the Freie Universität Berlin. Since 2008 he has been director of the Physical Chemistry department at the Fritz-Haber-Institute. His research focuses on the dynamics of elementary processes at surfaces, interfaces, and in solids, ultrafast dynamics in correlated materials, interfacial electron transfer, and photochemistry and vibrational spectroscopy at interfaces.

1.2. The Chemical Relevance of CO Oxidation

For a chemist interested in creating substantially more complex molecules, the simple reaction

$$2\,CO + O_2 \rightarrow 2\,CO_2 \tag{1}$$

carries little excitement. However, considering that this reaction requires three bodies to interact under highly specific energetic and geometric conditions for the reaction to occur homogeneously renders the understanding of the course of this reaction more interesting. From the standpoint of the electronic structure of the constituents the reaction is also spin-forbidden, as discussed in Section 6. The use of a catalyst may enable the reaction to occur through activation of the oxygen molecule near to the location of chemisorbed CO molecules, thereby allowing its spatiotemporal decoupled combination to give the product molecule CO_2. This provides the challenge of investigating the underlying elementary processes at an atomistic level and understanding the entire course of the reaction, including its complexity under reaction conditions.

CO is a redox-amphoteric molecule, and thus a valuable C_1 building block for synthesis reactions. This character is seen best in the water gas shift equilibrium:

$$CO + H_2O \rightleftharpoons CO_2 + H_2 \tag{2}$$

This reaction is of great practical relevance in both directions, either to generate hydrogen or to scavenge water from the reduction of CO_2, for example, in the synthesis of methanol. In the future the direct reverse water gas shift reaction will be of relevance in the chemical utilization of CO_2.[23]

Figure 1 shows an overview of the C_1 reactions in the C_1/H/O ternary system, excluding all reactions involving C–C bond formation. The formal oxidation state of carbon in these reactions is denoted. From this compilation it becomes apparent that CO is a most important building block in the C_1 reaction system. Both gas-phase species and adsorbates are indicated, and these may have a different isomeric structure on the surface and in the gas phase. It becomes clear that the reaction system becomes complex when the CO oxidation reaction is carried out in the presence of either water or hydrogen, even when they are only present as an impurity, which is relevant, for example, in high-pressure model studies. Although the chemistry of this system is complex, it becomes apparent that the choice of CO oxidation as a prototype

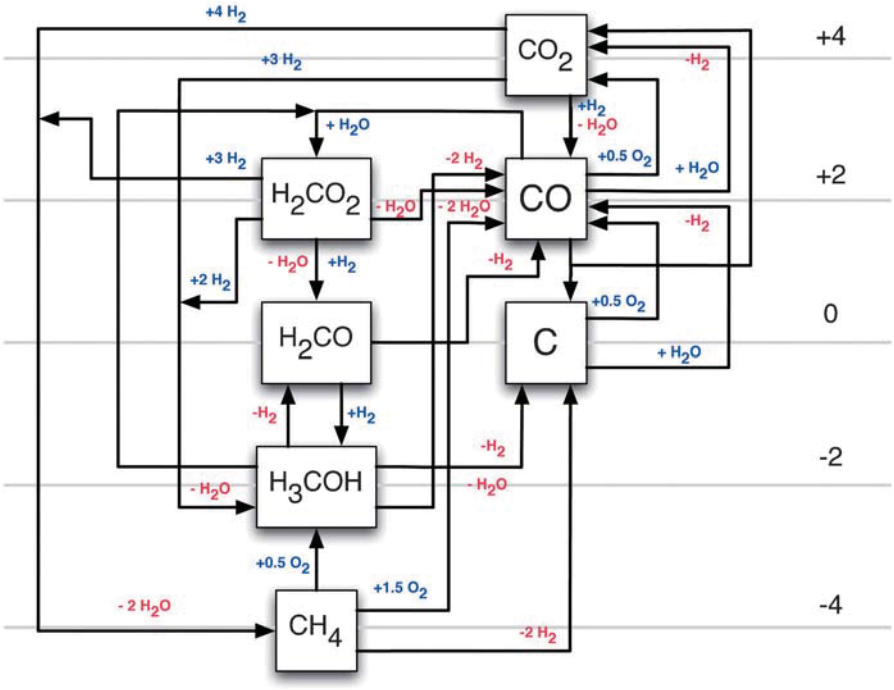

Figure 1. Selected reactions in the C1/H/O ternary system. The immense number of reactions involving C–C bond formations is omitted. The numbered lines denote the formal oxidation state of carbon in these reactions. Blue species are added to the reactants, while red species are liberated during reaction.

model reaction is motivated by the exclusion of multiple side reactions, which would complicate a rigorous mechanistic analysis. Extrapolating the results from such studies to reaction conditions where all the components of the system shown in Figure 1 are present may be dangerous when only incomplete reaction data are available. Such a situation is typical for "high-pressure" experiments on CO oxidation, where the other components can easily be present as impurities. Such experiments that bridge between surface science and high-performance conditions thus require utmost attention to keep the conditions truly comparable.

Strong effects from the transport of mass and energy in several dimensions of space additionally control the reaction rate under high-pressure conditions.[24] This precludes us from simply extrapolating results from atomistic studies that consider single-molecule trajectories to catalytic observations under real conditions. Precautions can be made to minimize the effects of transport limitations in macroscopic dimensions, but they cannot be removed from the kinetic process network. This leads to the occurrence of "gaps" between atomistic studies confined to two dimensions and observations under industrial conditions. Sometimes the gaps relating to reaction parameters and material composition are incorrectly generalized as gaps between surface science and catalysis science. The influence of transport in various dimensions of time and space is carefully studied in both sciences. It is an area of ongoing development to include transport phenomena in multiscale descriptions of catalytic reactions.[25] The failure to do so in the past was masked by various fitting procedures that led to unphysical values of certain model parameters. In the famous "bridging the gap" studies on ammonia synthesis these shortcomings are included in various parameters but it was always stated clearly there that it would not be the goal of the exercise to quantitatively predict high-performance data.[26] Mechanistically bridging over almost 10 orders of magnitude of pressure with an error of one order of magnitude is considered sufficient proof that the key elements of the reaction mechanism are correctly described. However, this view is not adequate for branched reaction pathways, which cannot be described with such a method today. This provides a strong incentive to improve our ability to unify concepts of chemical reactions between different regimes of parameters by using ab inito modeling.

The multiple uses of CO in reductive heterogeneous catalysis, such as Fischer–Tropsch chemistry, and the rich coordination chemistry of CO in homogeneous catalysis used in hydroformylation reactions is not considered here. It is clear, however, that a detailed understanding of the oxidation of CO is an important ingredient in understanding many relevant reactions that far exceed the frequently quoted application for car exhausts.

CO is furthermore a poison to many catalytic reactions involving transition-metal active sites because of its strong bonding with such sites that have unfilled electronic d states. For this reason CO abatement from incomplete combustion processes is a critical application. It is toxic to life and should not be released into the environment. In stationary sources of carbon combustion, such as blast furnaces or coal-fired power stations, elaborate processes for CO abatement (fuel economizers) are used to recover its chemical energy. In mobile sources, such as cars, it is important to minimize its emission under all conditions of operation. This is achieved in the car exhaust catalyst system by CO oxidation and by reaction of CO with NO:

$$2\,CO + 2\,NO \rightarrow N_2 + 2\,CO_2 \qquad (3)$$

It is clear that this reaction is hard to accomplish without the help of a reaction moderator that steers the reaction as indicated above.

1.3. The Use of CO Oxidation as a Probe Reaction

The use of CO oxidation as a probe reaction can either target the course of the reaction itself or the nature of the catalyst that brings about the reaction. The well-studied adsorption properties of CO on atomically well-defined

surfaces form a quantitative basis for both directions of research.[27] Adsorption geometries, adsorption enthalpies, and ample spectroscopic information collected over the last four decades form a reference library for studying systems more complex than extended single-crystal surfaces of metals. In addition, the high quality of the experimental data provided support for the evolution of theoretical surface science by providing reference data for method development and comparison of computational procedures. The development of accurate ab initio theoretical calculations and multiscale modeling allows predictions even for regimes of pressure and temperature which are difficult to access by experiment.[28,29]

A fundamental advantage of CO oxidation as a probe reaction is the fact that it is a reaction with one rate-determining step and a single product. The CO_2 product interacts much weaker with the surface metals than does the CO starting material. This renders the measurement and the interpretation of reaction data a facile exercise. The fact that the reaction occurs over a wide range of 13 orders of magnitude of pressures[30] allows further studies of a catalyst under a wide range of conditions to be performed.

Equations (4)–(6) describe the kinetically effective steps of the overall process.

$$CO_{gas} \rightarrow CO_{ads} \quad (4)$$

$$O_{2gas} \rightarrow 2\,O_{ads} \quad (5)$$

$$CO_{ads} + O_{ads} \rightarrow CO_{2,gas} \quad (6)$$

Only Equation (4) is an elementary step, the other reactions are composed reactions, where complex details of the dynamics of the dissociative adsorption of oxygen and the formation of CO_2 as well as its liberation into the gas phase remain unconsidered.

The reaction can be studied at pressures below 10^{-3} mbar not only by integral methods but also with spatiotemporal resolution.[31] These studies, pioneered by G. Ertl, provide fundamental insights into the dynamics of chemical reactions and into the phenomena of self-organization of chemical reactions.[12,32] The interplay of site blocking by strong adsorption of reactants and the liberation of these sites by reaction fronts moving over homogeneous parts of the surface creates the complex behavior of a simple reaction. The integral reaction rate is modulated through macroscopic coupling phenomena that give rise to unstable kinetics or in rare cases to regular kinetic oscillations. An elegant approach is the characterization of the spatiotemporal pattern formed at single-crystal surfaces or polycrystalline facets and their kinetic phase boundaries by in situ observation by photoemission electron microscopy (PEEM).[33]

With the wide range of experimental studies available and with a fairly mature theoretical picture of the course of the CO oxidation reaction it is also possible to extend the use of CO oxidation to probe the dynamics of chemical reactions. In such studies, the dynamics of the energy flow between reacting species and the catalyst surface are studied with a temporal resolution adequate to the elementary processes. These occur typically on ultrafast (femto- to picosecond) timescales.

Many catalyst surfaces undergo structural and chemical transformations in contact with reactants, particularly at higher pressures. It is possible that metal-to-oxide transitions occur and that substoichiometric compounds control the catalytic activity of a chemically simple catalyst. The prominent example of ruthenium (and its oxides) has been studied extensively by using CO oxidation as a model reaction.[34] The combined application of multiple experimental and theoretical tools has given a fairly complete picture of how a catalytic reaction can transform the structure and chemistry of an element surface.

In summary the chemically not so challenging reaction of the catalytic oxidation of CO presents many facets that makes it worthwhile for study in the context of a large array of topics in heterogeneous chemistry. The main value of these studies is a solid body of rigorously understood facts about the chemical and physical aspects of a chemical reaction that carries generic information about heterogeneous processes. At present, a detailed knowledge and control of the reaction has been gathered, but there still exist open questions on the material side. The dynamic nature of active catalysts may well require investigations of both the active material as well as the reaction mechanism. The use of ruthenium as a catalyst, as will be discussed below, is a good example of this new scientific approach. Here we illustrate that the chemical dynamics of the system provides feedback loops between the surface reactivity and reaction-induced modification of the catalyst surface. The frequently used approach to decouple material science from surface processes by applying low pressures and reaction temperatures is rather a borderline case and is not representative of a high-performance catalyst, where reaction conditions and nanostructuring create favorable conditions for feedback loops to operate between reactant and catalyst chemistry. What has also not been considered in detail is the atomistic dynamics of the reaction. Issues of electronic and motional coupling between surfaces and adsorbates and the dynamics of the underlying elementary processes in the ground and excited states are typically outside the scope of "chemical" considerations, but are essential for a fundamental understanding of the reaction.

This Review presents a multidisciplinary approach to research on various aspects of CO oxidation performed at the Fritz Haber Institute in Berlin. Instead of providing a comprehensive overview we wish to point out how complementary approaches can yield profound insights into this prototypical reaction by using selected methods with a wide variety of materials and reaction conditions. The following case studies will cover the state-of-the-art regarding the understanding of CO oxidation in a wide variety of systems ranging from molecular clusters, to metallic systems of various structures, and to complex oxides. Starting from spectroscopic investigations of finite systems in the gas phase in Section 2 and studies on the ultrafast dynamics of energy transfer in Section 3, the reaction is elucidated on well-defined supported model catalysts (Section 4). The use of CO oxidation as a probe reaction in high-performance catalysis is demonstrated in Section 5 for real systems with complex

structures. Theoretical studies on the CO oxidation reaction under realistic conditions of pressure and temperature and in the steady state are discussed in Section 6. From these examples it becomes clear to what level of resolution the understanding of a heterogeneous reaction can be carried and how many detailed insights into the structure of reactive solid interfaces can be evaluated by using the tool of CO adsorption/oxidation.

2. Spectroscopic Characterization and Reactions on Gas-Phase Clusters

Metal clusters can be seen as models for the surface of bulk materials, although in general the average atomic coordination in the cluster is much lower than on the surface. Therefore, this analogy works best for low-coordinate surface sites such as on corners and steps, as well as for adsorbed atoms. These sites are proposed in the classical picture of active sites as introduced by H. S. Taylor to be most relevant for heterogeneous catalytic reactions.[35] On the other hand, as already mentioned in the Introduction, small metal particles are themselves of direct interest for catalytic applications. A high dispersion leads to an increase in the activity because of the maximization of the active surface, and qualitatively new chemical properties also emerge for nanosized particles and clusters.[36] A striking example for the very different behavior of nanosized particles compared to that of the extended material is observed for gold;[37] in its bulk form, gold is proverbial for its inertness while in a highly dispersed form it is able to catalyze low-temperature oxidations, for example, the selective epoxidation of alkenes.[3,38] The activity of these gold particles is found to depend crucially on the support material and this interaction is presumed to also involve charge transfer between the support and metal particles.

These findings have triggered intensive investigations of the chemical and physical properties of transition-metal clusters—and of gold clusters in particular—in the gas phase. Two important goals of this research are 1) to understand the relationship between the structures of the clusters and their behavior, and 2) to investigate the chemistry occurring on the surface of the clusters. In principle, both aspects can be probed by vibrational spectroscopy. Conventional methods of absorption spectroscopy are difficult to apply, however, as the clusters have to be investigated in the gas phase under very dilute conditions in molecular beams or ion traps; in conventional absorption spectroscopy, the effect of the sample on the light is recorded and a sufficiently large line-integrated density of particles (in particles/cm^2) is needed to observe any signal. The alternative is to record the effect of the light on the sample; in this case a sufficiently large number of photons/cm^2, that is, a sufficient fluence, is needed to observe any signal. The effect of the light on the sample can, for example, be its ionization or fragmentation, and the resulting ions or ionic fragments can be mass-selectively detected. This so-called "action spectroscopy" thus provides high sensitivity and is selective for cluster sizes. The crux of "action spectroscopy" in the infrared (IR) region is, however, the need for widely tunable lasers with sufficient fluence to induce these processes, which often require the absorption of multiple photons. During the last two decades, the application of IR free electron lasers (FELs) has yielded new opportunities to record the vibrational spectra of gas-phase clusters, as demonstrated for a range of metal-carbide and -oxide clusters as well as clusters of transition-metal atoms and of complexes of these clusters with small molecules.[39]

2.1. Structural Characterization of Transition-Metal Clusters

The structural characterization of metallic clusters has greatly benefitted from the introduction of FELs as the infrared light source. Here, far-IR spectroscopy has in particular profited from the fluence available in the long wavelength range at the FELIX facility,[40] which has provided access to modes of low IR intensity, such as metal–metal vibrations. Additionally, spectroscopy in the gas phase allows for the detection of low-frequency modes that in the case of deposited or embedded clusters are often covered by vibrational bands related to the substrate.

The "messenger method" can be used to detect the absorption of far-IR photons. In this approach a weakly bound ligand is evaporated from the cluster complex upon absorption of one or a few IR photons. The basic assumption behind the application of this method is that only the metal cluster acts as the chromophore, while the weakly bound atomic or molecular ligand just acts as a messenger and does not perturb the structural properties of the cluster. This will be true for most transition-metal clusters complexed with rare gas atoms, since directional binding usually leads to significant barriers for isomerization. Indeed, the influence of the rare gas atom on the IR spectra has been found to be negligible in the case of cationic vanadium clusters.[41] It is found experimentally that the band positions in the IR spectra of complexes of V_n^+ with Ar, Kr, or Xe are essentially identical. However, slight shifts of the bands on the order of about 1–2 cm^{-1} per Ar atom can be observed in the spectra of complexes of a cluster with multiple argon atoms. For late transition metals such as Co, where rare gas atoms are more strongly bound, significant changes in the IR spectra are observed, depending on the number of rare gas atoms bound to the cluster.[42] The bonding of Kr atoms with small gold clusters has been investigated theoretically in detail, and will be discussed below.

In combination with density functional theory (DFT) calculations, the experimental IR (multiple) photon dissociation (IR-(M)PD) spectra allow for an unambiguous determination of the structure of the clusters in many cases. Starting initially with cationic clusters of Group 5 metals (V, Nb, Ta),[43,44] these studies have since then been extended to cationic clusters of late transition metals which are relevant in heterogeneous catalysis[42,45,46] and also to neutral clusters.[44,47–49] For certain clusters it has even been possible to obtain isomer-specific IR spectra by making use of the differences in their ionization potentials, that is, by selective ionization of the cluster/rare gas complex of a single isomer near the threshold.[49]

One major issue in these investigations is the need for adequate theoretical descriptions of the clusters. This is still, especially for larger clusters of the late transition metals, a challenging task because of their electronic configurations with open d shell and the large number of plausible isomers for the larger clusters. We hope that the availability of experimental data on the vibrational properties of metal clusters will stimulate further calculations and the development of theoretical methods that will lead to an improved understanding of the structures and dynamics of these species. The difficulties with the quantum-chemical methods available today become evident, for example, with rhodium clusters. Rh_8 clusters have previously been predicted to have a cubic structure, and larger Rh clusters are also suggested to retain the cube as its structural motif.[50] However, calculations by Wang and Johnson[51] on Ru_4 suggest that open square and cubic structures may be due to the treatment of electron-exchange correlation within density functional theory (DFT), when used with semilocal approximations to exchange correlation functionals. These effects may be reduced by the use of hybrid functionals, which include a portion of exact exchange.[51,52] Indeed, a global search of the potential-energy surface by using the basin-hopping approach coupled with density functional theory calculations identifies a slightly distorted cube as the global minimum if the commonly applied generalized gradient approximation is used, as implemented, for example, in the pure Perdew–Becke–Ernzerhof (PBE)[53] functional. If a portion of Hartree–Fock exchange is incorporated, as in the hybrid PBE1[53,54] functional, a very different result is obtained. The cubic isomer is now found 0.92 eV above the ground state, which has a bicapped octahedral structure.[45] Figure 2 shows that the close-packed bicapped octahedral isomer reproduces the experimental spectrum, while the cubic structure has a very different spectrum. The bicapped octahedral structure is very similar to the one for other 8-atom metal clusters, for example, of the Group 5 transition metals,[43b,d,44] or of cobalt.[42]

Similar difficulties are known to arise for gold clusters, where semilocal density functional theory tends to overestimate the stability of planar clusters.[55] Experimental information on their structures has been available in the past for charged gold clusters, for example, from measurements of their ion mobilities,[56,57] from trapped ion electron diffraction,[58,59] or from anion photoelectron spectroscopy,[60,61] and significant structural differences between singly charged cationic and anionic gold clusters have been identified.[62] The size at which the initially planar clusters start to form 3D structures strongly depends on the charge state. The use of the information obtained from vibrational spectroscopy of the neutral gold clusters[48] enables a complete picture of the charge state dependence of the structures to become possible. The charge-state dependence of the structures is illustrated in Figure 3 a) for the gold cluster containing seven atoms. In this case, the structure is different for all three charge states, although there is actually only a small amount of rearrangement between the neutral species and the anion. An increase in the electron density results in the average coordination of the gold atoms decreasing and the formation of more open structures. Tetrahedral structures have been found for larger anionic gold clusters, that is, Au_{19} and Au_{20},[60–62] and the IR spectra also identify these geometries unambiguously for the neutral clusters (see Figure 3 b).[48]

2.2. Bonding of Kr Atoms to Small Gold Clusters

When Kr is used as a messenger atom in IR-MPD experiments on neutral gold clusters, one has to realize that a partially covalent Au−Kr bond is formed. With a binding energy of a few tenths of an eV (0.1–0.2 eV per Au-Kr bond according to DFT-GGA, 0.2–0.3 eV according to MP2 and CCSD(T)), these bonds are relatively weak. Nevertheless, this implies that 1) the Kr atoms are localized at a specific

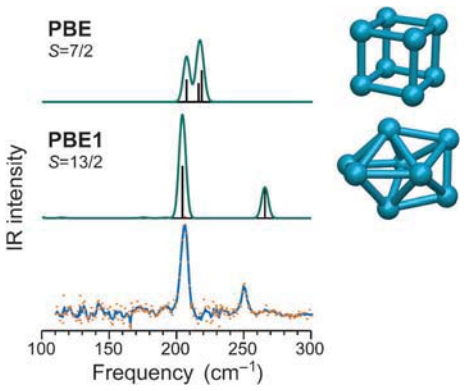

Figure 2. Experimental far-IR spectrum of Rh_8^+ (bottom) compared to the predicted IR spectra for the global minimum structures obtained using either a pure functional (PBE) or by including exact exchange with a hybrid functional (PBE1). (From Ref. [45].)

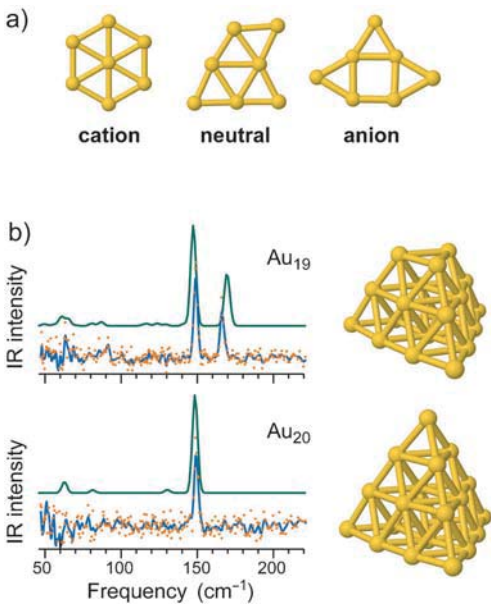

Figure 3. a) The structures of gold clusters containing seven Au atoms vary for the different charge states. b) Comparison of the experimental and calculated IR spectra for Au_{19} and Au_{20}. (From Ref. [48]).

bonding site at finite temperatures, that 2) the vibrational spectrum of each of the Au_nKr_m clusters can be rather different from that of the bare Au_n cluster, and that 3) the energy ordering of the Au_nKr_m isomers can be different from that of the corresponding bare Au_n isomers.[63] The influence of the Kr atoms is particularly prominent for the vibrational mode of the dimer, which becomes IR active when one or two Kr atoms are attached. Generally, the effect of the covalently bound Kr atoms on the vibrational spectrum is a change in the relative line intensities, the activation of modes (arising from symmetry lowering) that are IR-inactive in the bare cluster, and the appearance of new modes in the low-frequency part of the spectrum (30–100 cm^{-1}) that involve the motion of the Au and Kr atoms.

The free-energy surface of gold clusters of a given size is rather shallow in the region between different local minima, and many isomers are often found very close in energy. A change in the relative energy of the isomers upon complexation occurs, for example, with Au_3; the bare cluster exists in two isomers, an obtuse-angle and an acute-angle triangle, with an energy difference of about 0.1 eV. Thus, only the lowest energy isomer is expected to be present in a system in equilibrium at approximately 100 K. When one or two Kr atoms are attached, the overall binding energy of the two isomers becomes almost the same, because Kr binds more strongly to the less-stable isomer. The measured IR-MPD spectrum of Au_3Kr_2 can indeed only be fully explained if both isomers are assumed to be present. Two isomers that are almost degenerate in energy are found for Au_4, and their energy difference becomes even smaller when a Kr atom is attached; in this case, both isomers are also concluded to contribute to the observed IR-MPD spectrum.

For clusters larger than Au_4, the strength of the Au–Kr covalent bonding is reduced, while the van der Waals interaction becomes stronger. At finite temperature, Kr is then somewhat delocalized around the cluster and its influence on the vibrational spectrum is almost negligible. This interpretation is made possible by considering the finite temperature spectrum as coming from a thermostatted molecular dynamics simulation, that is, by going beyond the analysis of the harmonic spectrum with Kr localized on a very weak binding site. From these simulations we also find that bare gold clusters can undergo an internal transformation at temperatures as low as 100 K. Neutral Au_7, for example, can transform through breaking a bond of the internal rhombus (see Figure 3 a), passing through the shape of the ground state anion (which is a saddle point for the neutral cluster), and subsequently forming the bond that corresponds to the opposite diagonal of the rhombus. This transformation, which appears in the thermostatted molecular dynamics trajectory of the cluster, is reflected in the theoretical finite-temperature spectrum, and might explain the observed broadening and splitting in the highest frequency peak of the IR-MPD spectrum of Au_7.[64] As another example, Au_{14} can be thought of as a triangular prism surrounded by a planar ring that is only loosely bound to the prism. Its free-energy surface is so shallow that, at low temperature, the molecular dynamics trajectories reveal a motion of the internal prism relative to the ring.[64]

2.3. Interaction of Single CO Molecules with Transition-Metal Clusters

As mentioned in the introduction, CO is a common probe molecule for the investigation of surface sites and its oxidation is used as a model reaction for more complex (catalytic) oxidation reactions. Such catalytic oxidation cycles have also been reported for cluster systems.[65,66] Our intention is to obtain a detailed understanding of the interaction of CO with transition metals and to investigate how this depends on the metal, cluster size, and charge state.

The reaction of CO with a transition-metal surface can lead to two fundamentally different products: a molecular adsorbate or the products of its dissociation, namely, separated atomic O and C species. The fate of the CO molecule highly depends on the metal, its surface structure, and the reaction conditions. Vibrational spectroscopy provides a convenient method to distinguish between these two reaction channels not only for extended surfaces but also for isolated cluster complexes. From the study of cluster complexes of CO at low coverage it appears that there is actually little difference between small clusters and extended surfaces.[67] The transition from dissociative to molecular adsorption closely follows the diagonal line through the periodic system already described by Brodén for the binding of CO to metal surfaces at ambient temperatures (Figure 4).[68] Early transition metals such as V, Nb, or Ta bind CO dissociatively, while the late transition metals binds CO exclusively as a molecular ligand. Only for neutral tungsten is a size-dependent binding behavior found. For clusters containing 5, 7, 8, 9, or 11 W atoms the appearance of the ν(CO) band indicates the presence of intact CO molecules as ligands, while such a band is missing for larger W clusters, thus indicating dissociative binding, as also found for W surfaces.[69] Tungsten is the only case that shows an apparent cluster-size effect, and it is remarkable that no fundamental difference in the binding behavior of CO has been observed in the cases of metals where clusters with different charge states have been studied.

21 Sc	22 Ti	23 V C	24 Cr	25 Mn	26 Fe N	27 Co ANC	28 Ni NC	29 Cu	30 Zn
39 Y	40 Zr	41 Nb N	42 Mo	43 Tc	44 Ru A C	45 Rh ANC	46 Pd A C	47 Ag NC	48 Cd
57 La	72 Hf	73 Ta N	74 W N	75 Re C	76 Os	77 Ir N	78 Pt ANC	79 Au ANC	80 Hg

Figure 4. Overview of the binding behavior of CO on transition-metal clusters as determined by IR-MPD spectroscopy in the gas phase. Orange fields denote elements where no ν(CO) band is observed, that is, where CO is dissociatively bound to the clusters. Blue shaded elements are those where the ν(CO) bands are indicative of CO molecules bound on-top. The blue/green fields indicate metals where in addition to binding on-top CO ligands are also found in higher coordination configurations. Experiments were performed on clusters in different charge states: anions (A), neutral species (N), or cations (C). (Reproduced from Ref. [67]).

The transition from dissociative to molecular binding of CO to metal surfaces can be understood from the fact that moving to the left in the Periodic Table of the elements results in a rise of the Fermi level and of the diffuseness of the d orbitals. This leads to a higher electron density in the C–O antibonding 2π orbital and eventually to dissociation.[70] Quantum mechanical calculations reproduce this trend,[71,72] which seems to also hold qualitatively for gas-phase clusters. However, this picture is oversimplified since the Fermi level determines the work function, which translates into the ionization potential (IP) of an isolated cluster. It is well-known that clusters show pronounced size-dependent variations in their IP, which, within this model, would contradict the size independence of ν(CO) for CO adsorbed on neutral clusters.

An important aspect in the study of adsorbed CO molecules is the strong sensitivity of the frequency of the internal CO stretching vibration ν(CO) to 1) the electron density at the metal center and to 2) the binding geometry of the CO molecule. This sensitivity and the large oscillator strength of CO ligands, which allows for vibrational spectroscopy even at very low coverage, is the reason for the wide use of CO adsorbates for probing the properties of metal surfaces or of finely dispersed metals through ν(CO).[73]

The bonding of CO to transition-metal atoms is commonly described in terms of the Blyholder model of M←C σ donation and M→C π backbonding.[74] As the amount of backbonding is related to the occupancy of the M(d) orbitals, the internal CO bond strength, and thereby the ν(CO) frequency, depends on the charge on the metal center. Analogously, the interaction of a CO molecule with multiple metal atoms leads to a more efficient M→C π back donation and to significant weakening of the CO bond, typically leading to a decrease in the ν(CO) frequency by 100–150 cm^{-1} per additional metal–carbon bond. These shifts in the ν(CO) frequency allow the presence of CO ligands in an on-top (μ^1), bridging or (μ^2), or capping (μ^3) configuration to be identified. A pronounced cluster-size dependence in the binding geometry of CO is found for single CO molecules bound to rhodium cluster cations, neutral species, or anions (Figure 5).[75] At low coverage, that is, with only a single CO ligand bound to the cluster, only μ^1-CO is observed for the 3d transition metals, while CO can bind with higher coordination to 4d and early 5d transition metals (Figure 4). The μ^1 configuration again becomes more stable for late 5d (Ir, Pt) elements because of relativistic effects.[67,76] Overall, this behavior is very similar to the observations for extended surfaces.

In the gas phase, metal-cluster complexes can be prepared in different charge states and the charge dependence of ν(CO) van be directly observed (Figure 6). The charge and cluster-size dependence of ν(CO) can be modeled by assuming that the charge of the cluster is equally distributed over all the surface metal atoms in the cluster.[77] This fractional charge at the CO binding site is reflected in the M(δ) occupancy and leads to a change in the occupancy of the antibonding CO(2π) orbital, thereby affecting the C–O bond strength. The solid lines in Figure 6 are obtained from a quantitative model that accounts for the influence of a diluted

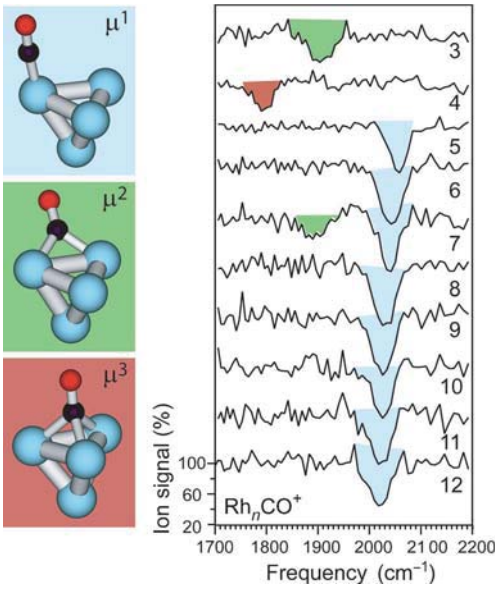

Figure 5. IR absorption bands of CO bound to cationic rhodium clusters of different sizes. Most Rh clusters bind CO in an on-top (μ^1) geometry, while bridging (μ^2) and face-capping (μ^3) binding geometries are also observed for smaller clusters.

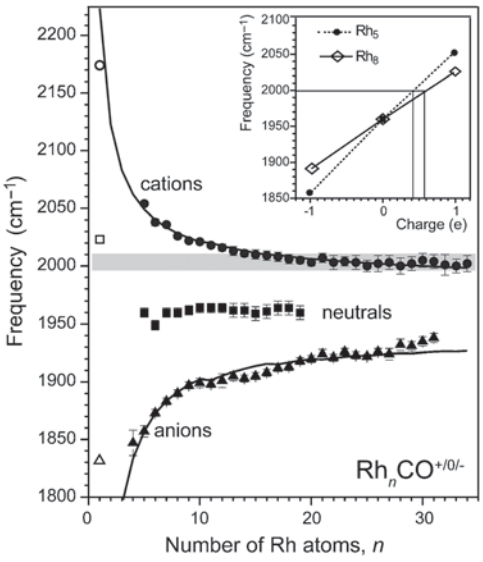

Figure 6. Effect of cluster charge and size on the CO stretching frequency for CO bound to rhodium clusters.[75,77] The values that are observed for ν(CO) on extended surfaces at low CO coverage are indicated by the gray bar. The inset shows a comparison with values of ν(CO) for similarly sized clusters deposited on highly ordered Al_2O_3 (horizontal line).[78]

charge. The model successfully describes the size dependence of ν(CO) for the CO complexes of rhodium, cobalt, and nickel clusters. However, in the cases of the charged clusters, the asymptotic values ν_∞(CO) for $n\rightarrow\infty$ do not exactly coincide with those for the neutral clusters. This may indicate that the charge is partially localized at the binding site. Furthermore, the ν(CO) values for the neutral clusters and the asymptotic

values ν_∞(CO) are significantly below the values of ν(CO) found for CO adsorbed on extended surfaces (low-coverage limit). This is probably related to the lower coordination of the cluster atoms compared to an extended surface.

The vibrational data for CO adsorbed on free clusters in the gas phase can be compared to vibrational data of CO adsorbates on a substrate to assess the electron density on the deposited metal particles. Quantitative information on the charge transfer between the metal cluster and substrate, for example, from defect centers, can be derived in this way. However, in such a comparison one has to be aware that structures of deposited clusters can be different from those in the gas phase and that, because of a strong dependence of ν(CO) on the surface coverage, a comparison can only be made for similar coverages, that is, at the low-coverage limit. Additionally, CO adsorption itself may induce changes in the charge distribution between the metal and support.[79] A comparison of deposited Rh clusters on a highly ordered Al_2O_3 film[78] with the gas phase data indicates a significant positive charging of the deposited clusters by about $+0.4$ to $+0.6\,e$.[75] Similar reasoning has been used to assess the charging of small gold clusters deposited on defect-rich or defect-free MgO substrates.[80]

Finally, CO binding can also be altered by coadsorbed species. For example, hydrogen/CO coadsorption on transition-metal clusters has been studied in more detail because of the relevance of this system to the Fischer–Tropsch synthesis. The hydrogen binds dissociatively on most transition-metal clusters.[81] The hydrogen coverage can alter the CO binding in different ways. For example, site blocking by hydrogen atoms can lead to the molecular binding of CO to metals at which it would normally dissociate, such as is observed for vanadium.[82] More subtle changes are due to the electron localization in the M–H σ bonds which lead to a reduction in the electron density available for backdonation to the CO(2π) orbital. Here, a close to linear dependence of the shift of ν(CO) on the hydrogen coverage is observed for cobalt clusters and leads to a strengthening of the C–O bond with increasing hydrogen coverage. Comparing these shifts with the ν(CO) values for clusters in different charge states (see above) allows the amount of electron transfer to coadsorbed hydrogen ligands to be quantified. This ranges from 0.09 to 0.25 electrons per hydrogen atom for clusters with 4–20 Co atoms.[83] As ν(CO) is sensitive to the relative coverage, that is, the ratio of coadsorbed hydrogen atoms to the number of surface metal atoms, this concept of probing electron localization can also be extended to larger particles and might even be applicable to extended surfaces.

A similar example that demonstrates the importance of ligand coadsorption effects is given by the adsorption of CO and O_2 on free gold clusters, which we have investigated theoretically in the framework of the catalytic CO oxidation reaction. Neutral gold clusters have been modeled in a gas-phase atmosphere containing CO and O_2 in variable compositions in the 100–600 K temperature range by means of DFT calculations in conjunction with the ab initio thermodynamics technique.[84] When CO adsorption and O_2 adsorption processes are compared, gold clusters are found to have a strong preference towards binding CO rather than O_2. However, if both ligands are simultaneously present in the gas phase, thereby embedding the cluster, a cooperative adsorption effect takes place and the preferred products are the ones including both CO and O_2. Among these products, some are found to contain stable species such as CO_2 and CO_3 as adsorbed ligands. These cluster-plus-adsorbate structures are plausible intermediates in the catalytic CO oxidation reaction.

3. Ultrafast Reaction Dynamics Induced by Femtosecond Laser Excitation

While the preceding section focused in detail on structural details in well-defined finite model systems we will now address the reaction dynamics and role of energy and charge transfer between the reactants and a metal substrate. Chemical reactions usually occur in the electronic ground state, where the reaction barriers are overcome by thermal activation. Exceptions from this rule are photoinduced or electron-stimulated processes, where the activation is mediated by electronic excitation to an excited state, which initiates a nuclear motion along the reaction pathway. Examples are photochemical processes and chemical reactions induced by electron attachment or charge transfer. A key concept of chemical reaction dynamics relies on the Born–Oppenheimer (BO) approximation, in which electrons are assumed to follow the nuclear motion instantaneously and thus the reaction evolves adiabatically on a Born–Oppenheimer potential-energy surface (PES).[85] Thereby, non-adiabatic coupling effects between the nuclear motion and the electronic degrees of freedom are neglected. This assumption, however, is only valid if the involved electronic state and PESs do not approach each other significantly. In the case of conical intersections, the crossing of two PESs at a certain nuclear configuration leads to coupling between different electronic states and to the breakdown of the BO approximation near the conical intersection.[86] A similar situation exists at metal surfaces, where a continuum of electron/hole pair excitations in the metal leads to a whole manifold of close-lying PESs, which are spaced by the electron/hole pair excitation energy. It can, therefore, be expected that for chemical reactions or adsorption/desorption processes at metal surfaces, which are accompanied by such electronic excitations in the substrate, a breakdown of the BO approximation and a coupling between the electronic and nuclear degrees of freedom may occur.[87] Examples for such processes are the emission of so-called exoelectrons and chemiluminescence during the oxidation of alkali metals (caused by the release of energy which is transferred into light emission) or in the scattering of highly vibrationally excited molecules at metal surfaces.[88] Further examples of non-adiabatic effects at metal surfaces include the relaxation of the vibrational energy of chemisorbed molecules and energy dissipation in dissociative adsorption. The excess energy is thereby transferred from the reactants to electronic excitations (e.g. photons and exoelectrons as well as electron/hole pairs and plasmons in the substrate). Hot electrons excited in the substrate can be detected as a chemicurrent across the

Schottky barrier between a thin metal film and an n-type semiconducting substrate.[89]

Starting from a well-defined state of adsorbed molecules (or atoms) at a metal surface, such non-adiabatic reaction dynamics can also be induced by femtosecond (fs) laser excitation.[90] Figure 7 illustrates schematically the possible pathways of energy flow in femtochemistry at a metal surface.[91] Absorption of an intense fs laser pulse generates a transient non-equilibrium distribution of hot electrons, which leads to an electron temperature exceeding the lattice temperature by several thousand degrees Kelvin on a fs timescale. Non-adiabatic coupling of this electronic transient to adsorbate vibrational degrees of freedom can induce processes such as desorption or reactions between coadsorbed species.[92] The distribution of the hot electrons on the metal surface subsequently cools down by diffusion into the bulk and by electron–phonon (e-ph) coupling to the lattice. This gives rise to an increase in the phonon temperature, which can also mediate chemical reactions of adsorbates through thermal activation. Direct photoexcitation of the adsorbate can, however, be neglected in (optically) thin atomic or molecular layers.

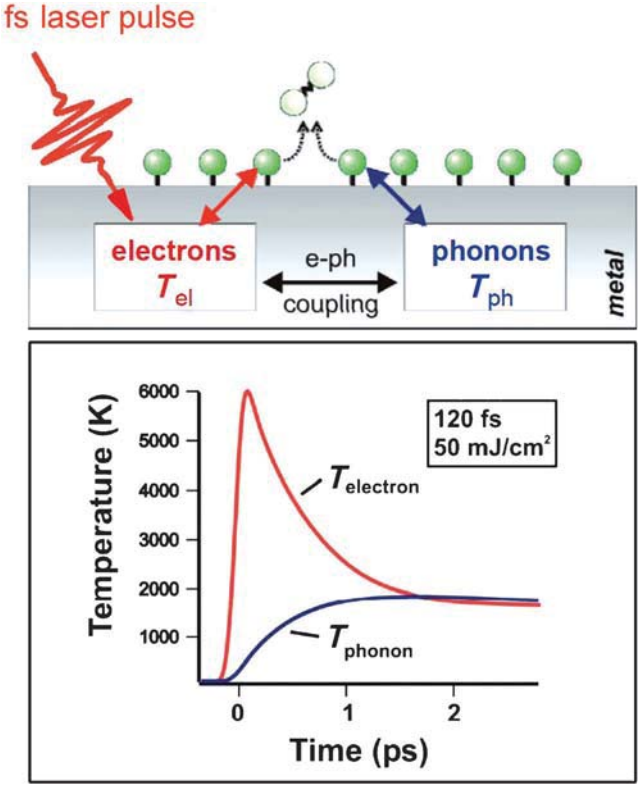

Figure 7. Surface femtochemistry at a metal surface. Top: Schematic diagram of the energy flow after femtosecond (fs) laser excitation. A fs laser pulse excites the electronic system of the substrate, which then equilibrates with the lattice phonons by electron–phonon coupling on a time scale of picoseconds (ps). Surface reactions can be driven either by non-adiabatic coupling to the photoexcited hot electron distribution, which is characterized by the electron temperature T_{el}, or by activation with lattice phonons of temperature T_{ph}. Bottom: Temperature transients for a Ru metal substrate for the electron and phonon heat baths with temperatures T_{el} and T_{ph}, respectively, calculated with the two-temperature model for an exciting laser pulse of 120 fs and 50 mJ cm^{-2} at 800 nm center wavelength.

The key point in femtochemistry at metal surfaces is that, within a time span shorter than the e-ph coupling time, both the electron and phonon heat baths are far out of equilibrium (i.e. the electronic system is highly excited and provides "hot" electrons, while the lattice is comparatively "cold").[87] This provides the opportunity to induce and study non-adiabatic reaction dynamics within this time span (typically ca. 1 ps) and separate such processes from near equilibrium reactions, which are induced thermally and can be described within the BO approximation. As surface femtochemistry is induced by an impulsive laser excitation, various methods of time-resolved laser spectroscopy can be used to study the dynamics of the underlying elementary processes and to identify the mechanisms and time scales of energy flow between the different degrees of freedom. For example, the time evolution of the electronic structure and e-ph coupling can be probed by time-resolved photoelectron spectroscopy,[93,94] while the vibrational dynamics of the reactants during the reaction can be analyzed by sum-frequency generation spectroscopy.[95]

3.1. Femtosecond Laser-Induced CO Oxidation on Ru(001)

In the following we discuss the fs laser-induced oxidation of CO on Ru(001) as an example of non-adiabatic reaction dynamics at a metal surface. The oxidation of CO on ruthenium and ruthenium oxide surfaces has received considerable attention as an important model system for heterogeneous catalysis. Under high-performance reaction conditions the CO oxidation will occur on an oxide surface[19] (which is thermodynamically favored at high temperature and oxygen pressure[20]), while under ultrahigh-vacuum (UHV) conditions the metallic elemental Ru surface is thermodynamically stable. Here we focus on the well-defined (2×1)-O/Ru(0001) surface onto which CO has been coadsorbed at 100 K up to saturation (for details see Ref. [97]). It is important to note that in this system CO_2 cannot be formed thermally under UHV conditions (i.e. by heating the surface) as a result of the remarkably high Ru–O bond strength (4.9 eV/molecule). If CO_2 formation can be induced under such conditions by fs laser excitation, a new reaction pathway is opened up which is not accessible under equilibrium conditions.

Figure 8 demonstrates both the desorption of CO and the formation of CO_2 induced by fs laser excitation of the CO/O/Ru(001) surface.[97] The first shot yield of CO and CO_2 increases nonlinearly with absorbed laser fluence ($Y \approx F^3$), with a branching ratio between CO desorption and oxidation of $Y(CO)/Y(CO_2) \approx 35$. The nonlinear dependence of the reaction yield on laser fluence is consistent with a substrate-mediated excitation mechanism as discussed below. Time-of-flight spectra (Figure 8 inset) reveal that the translational energy of the CO_2 products ($E_{trans} = 1590$ K) is substantially higher than for desorption of molecular CO ($E_{trans} = 640$ K). The observed differences in the translational energies of the reaction products can have a different origin: On the one

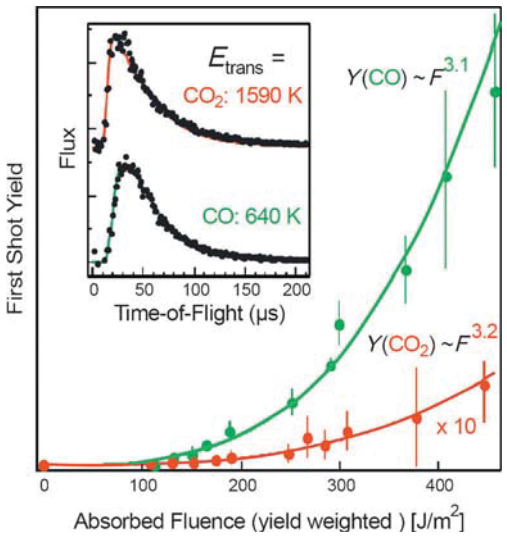

Figure 8. Femtosecond laser-induced desorption and oxidation of CO on a (2×1)-O/Ru(001) surface: The first shot yields of the desorbing CO and CO_2 reaction products depend nonlinearly on the absorbed fluence F of the 800 nm, 110 fs laser pulses. The solid lines represent fits to a power law F^n with exponent $n \approx 3$. Inset: Time-of-flight distributions reveal a significantly higher translational energy for the CO_2 molecules compared to desorption of CO. (From Ref. [97])

hand a different (phonon- versus electron-mediated) excitation mechanism can result in a different energy transfer into the translational degrees of freedom of the desorbing products (because different electronic states are involved). On the other hand a barrier in the ground state PES for the CO + O reaction could govern the dynamics and energy partitioning of the reaction for CO_2 formation. However, before this question can be addressed, the excitation mechanism for the CO desorption and oxidation process must be known.

A direct way to obtain insight into the dynamics of the underlying excitation mechanism and to differentiate between electron- and phonon-mediated reaction pathways is provided by two-pulse correlation measurements, which exploit the different response times of the electronic and phonon systems of the metal substrate upon fs laser excitation (see Figure 7). In these experiments, the adsorbate-covered surface is excited by two cross-polarized pulses of nearly equal intensity and the reaction yield is measured as a function of the pulse–pulse delay.[92,97] As a consequence of the nonlinear fluence dependence of the reaction yield (see Figure 8), the width of the two-pulse correlation will depend critically on the excitation pathway. A narrow full-width at half-maximum (FWHM) of the order of the e-ph coupling time is a clear indication for an excitation mechanism whereby the transient hot electron distribution couples non-adiabatically to the adsorbate, since only for pulse–pulse delays shorter than the e-ph equilibration time, is the electron temperature significantly enhanced due to the combined effect of both excitation pulses.[92] In contrast, a phonon-mediated process proceeds typically on a much slower time scale of tens of picoseconds because of the significantly longer energy storage time of the lattice compared with the electronic system and the slower coupling time of the phonon bath to the reaction coordinate. It is important to note that on these time scales excited electronic states of the adsorbate–substrate complex have decayed and the electronic and phonon systems have equilibrated. Hence, the reaction will proceed electronically adiabatically on the electronic ground state PES. We may thus also call the latter type of process "thermally activated" reactions, because on the corresponding time scales the different subsystems of electrons, phonons, and adsorbate vibrations are nearly equilibrated.

Figure 9 shows the result of such two-pulse correlation measurements for the CO/O/Ru(001) system. It is remarkable that the time response observed for the CO desorption and oxidation reaction differ by almost one order of magnitude. The ultrafast response time (3 ps FWHM) obtained for the formation of CO_2 strongly suggests a reaction mechanism based on non-adiabatic coupling to hot electrons, whereas the much slower response of 20 ps for CO desorption indicates a thermally activated process by coupling to phonons.

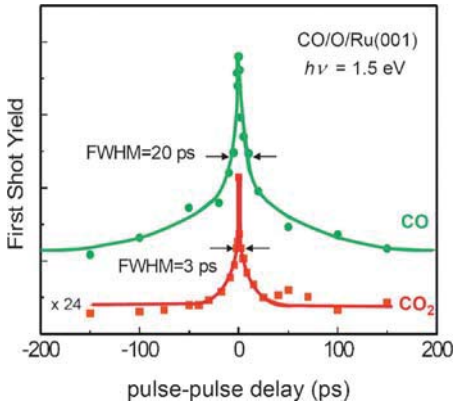

Figure 9. Two-pulse correlation measurement in the fs laser-induced CO desorption and oxidation from a CO/O/Ru(001) surface (800 nm, 110 fs laser pulses, ≈250 mJ cm^{-2} absorbed fluence): The full widths at half-maximum (FWHM) indicate that the CO_2 formation is induced by a hot electron driven process, while the CO desorption is thermally activated by phonons in quasi-equilibrium with the electronic system). (From Ref. [97].)

A quantitative analysis of the excitation mechanism and theoretical description of the energy transfer from the laser-excited substrate to the reactants in the adsorbate layer can be obtained by using a model based on frictional coupling between the electron and/or phonon heat bath to a harmonic oscillator that represents the adsorbate motion (reaction coordinate). Details of this procedure can be found in Ref. [98]. For the CO oxidation the two-pulse correlation trace as well as the fluence dependence are well-reproduced by assuming a pure electronic friction model with an ultrafast coupling time of 0.5 ps and an activation energy of 1.8 eV. In contrast, the CO desorption process can be described using the activation energy of 0.83 eV obtained from thermal desorption spectroscopy and a coupling time of a few ps to the phonon heat bath. Thus the fs laser-induced CO

desorption can be regarded as a "thermal" process. This quantitative analysis thus fully confirms the conclusions about the excitation mechanism of the two processes obtained from inspection of the two-pulse correlation measurements.

Further insight into the mechanism of the CO oxidation can be obtained from isotope effects. For an electron-driven mechanism, the short lifetime of electronic excitations at metal surfaces leads to a competition between the mass-dependent acceleration on the excited state PES and the relaxation back to the ground state. The observation of an isotope effect confirms not only that a particular surface process is electron-mediated, but also offers the opportunity to determine the rate-limiting step in a bimolecular reaction such as the fs laser-induced CO + O reaction. A remarkably high isotope effect was found on using a 50/50 mixture of ^{16}O and ^{18}O to prepare a $^{16}O/^{18}O/CO$ coadsorption system (with a yield ratio of $Y(^{16}OCO)/Y(^{18}OCO) \approx 2.2$). In contrast the isotope substitution of the CO reactant did not yield an isotope ratio that was significantly different from unity. These findings clearly demonstrate that the activation of the Ru–O bond is the rate-determining step in the CO oxidation reaction on Ru(001). Furthermore, electron-temperature-dependent DFT calculations[97,99] for a (2×1)-O/Ru(001) structure identify an unoccupied electronic state located approximately 1.8 eV above the Fermi level, which is antibonding with respect to the Ru–O bond. As the electron temperature increases, this state becomes partially occupied and thus the Ru–O equilibrium distance increases. This softening of the Ru–O bond provides a microscopic mechanism of the electron-mediated activation in the CO + O reaction on ruthenium.

Having identified the mechanism of CO oxidation in surface femtochemistry on ruthenium we finally address the question of how fast the reaction evolves in real time and how the energy is channeled into different degrees of freedom of the reaction products. The friction model discussed before provides a quantitative description of the coupling between the electronic system or the phonons of the substrate to a one-dimensional (1D) adsorbate coordinate, which is associated with the reaction coordinate.[93] The model was originally developed to describe femtosecond laser-induced desorption of diatomic species along the center-of-mass coordinate, which can be reduced to a 1D problem. However, the CO + O oxidation reaction clearly evolves on a multidimensional PES and it is not clear why a 1D model should be appropriate for an associative desorption reaction. Nonetheless, the 1D model has been applied with great success to the CO + O oxidation[97] as well as the H + H recombination reaction on Ru(001).[100] It should also be noted that the friction model yields the time evolution of the adsorbate temperature, which should, however, not be confused with the time required to complete the reaction, as the latter may include a complex motion on a multidimensional PES.

3.2. Multidimensional Dynamics

To gain further insight into these questions a detailed analysis of the multidimensional reaction dynamics is necessary. On the experimental side, this would require the measurement of the energy partitioning into translational, rotational, and vibrational degrees of freedom of the desorbing reaction products. On the theoretical side, such an analysis has to address the multidimensional dynamics under the influence of frictional coupling to the laser excited electronic and phonon system of the substrate. So far, such a complete analysis could only be performed for the associative desorption reaction of hydrogen ($H + H \rightarrow H_2$) on Ru(001).[101,102] We will, therefore, briefly summarize the main conclusions of this study and discuss these findings in the context of the CO + O oxidation reaction.

The fs laser-induced associative desorption of hydrogen, that is, the recombination of two hydrogen atoms from Ru(001), is mediated by electronic friction (analogous to CO oxidation on Ru).[101] The dynamics of this reaction have been comprehensively studied using rovibrational state-selective detection as well as ab initio theoretical modeling.[102] The desorbing hydrogen molecules exhibit a rather low excitation of the vibrational degrees of freedom (in comparison to the translation) and even less in the rotations. Thus, the energy is predominantly channeled into the translational degree of freedom, with an energy ratio among the translation, vibration, and rotation scaling as 5.4:1.3:1. An explanation for the substantial higher translational energy compared to the vibration has been given by Luntz et al. using molecular dynamics calculations with electronic frictions.[101b] The electronic friction coefficients were derived from time-dependent DFT calculations. For a given laser fluence (and hence time evolution of the electron temperature), classical trajectories were run in a molecular dynamics simulation on a 2D PES comprising the interatomic distance d (i.e. the H–H bond length), and the center-of-mass distance from the surface z. By evaluation of an appropriate number of trajectories which successfully led to desorption, the main experimental results (two-pulse correlation, nonlinear fluence dependence, and isotope effects) could be reproduced with remarkably good agreement.

Figure 10 (top) shows an exemplary trajectory for the formation of an H_2 molecule overlaid onto the 2D contour plot of the PES. Inspection of such individual trajectories indicates that the frictional coupling to the laser-excited hot-electron distribution leads initially to a preferential excitation of the vibrational coordinate, however, the rapid energy exchange ("thermalization") between the d and the z coordinate along the trajectory on the way to desorption conserves little memory of the mode of excitation. The unbalanced energy partitioning between translational and vibrational degrees of freedom observed in the experiment is found to originate predominantly from the topology of the ground-state PES, in particular from the small but distinct barrier in the translational channel. Thus, the ground-state topology causes this difference in energy partition rather than a preferential frictional coupling to one or the other coordinates. Considering the short excited-state lifetimes at metal surfaces, it is highly likely that the observed differences in the translational energies of the CO and CO_2 products of the CO + O reaction are also governed by the dynamics on the respective ground-state PES. However, the lack of

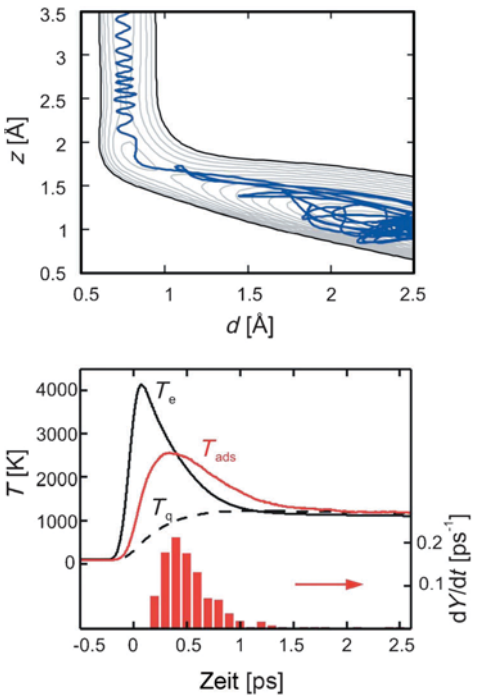

Figure 10. Dynamics of surface femtochemistry simulated by molecular dynamics with electronic frictions for the reaction of H + H→H_2 on Ru(001). The top diagram shows a typical trajectory on a 2D elbow type potential energy surface (d: interatomic H-H distance; z: center-of-mass distance to surface, contour plot of the 2D PES with 0.1 eV energy intervals). The bottom diagram shows the time evolution of the electron, lattice, and adsorbate temperatures as well as the desorption rate as a function of time after the excitation pulse. (From Ref. [101b].)

information about the vibrational and rotational excitations of the desorbing CO_2 molecules hinder us from drawing further conclusions about the topology of the ground-state PES.

The analysis of such trajectory calculations allows conclusions to be drawn about how fast the laser reaction proceeds, as demonstrated in Figure 10 (bottom). Here a histogram of successful desorption events as a function the time after excitation shows that the reaction is complete after a characteristic time span of approximately 0.5 ps (in the case of hydrogen formation on Ru(001)). As there is a finite coupling time from the electrons to the adsorbate coordinate, the reaction is clearly delayed and proceeds predominantly on the electronic ground-state PES, which governs the dynamics of the reaction products.

In summary, in this section we have demonstrated that chemical reactions at metal surface can be induced by electronic non-adiabatic coupling to electronic excitations in the substrate. In the case of the CO oxidation on the metallic Ru(001) surface, the electronic excitation allows activation of a reaction which does not occur under equilibrium conditions. Femtosecond laser excitation provides an "ultrafast trigger" of such reactions, which mediates the reaction by electronic excitations and non-adiabatic coupling on a sub-picosecond time scale. However, the dynamics of the reaction products are governed by the forces imposed by the ground state.

4. CO Oxidation on Supported Model Catalysts

Technically employed disperse metal catalysts consist of metal nanoparticles, which determine the catalytic activity, that are anchored onto a morphologically complex mixed oxide support.[102,103] Almost always, their preparation proceeds by wet impregnation from solution. The particles formed are not homogeneous in size and distribution, and are usually characterized by electron microscopy and their chemical reactivity. The catalytic activity is determined by the surface structure, which is difficult to access by surface physics techniques, since most materials are insulators. This prohibits the use of techniques involving electrons and ions as information carriers.[104,105] The use of thin, well-ordered oxide films as support materials, which do not charge up during measurement, provides an ideal solution to this problem, and allows us to capture some of the complexity represented by technically employed disperse metal catalysts while allowing the application of surface science methods to study surfaces at atomic detail.

There are two classes of model systems: In the first case, the goal is to represent a disperse supported metal or a mixed oxide catalyst.[6,104–109] The first type is based on the ability to model the bulk or volume of a supporting oxide by using thin film techniques. In a second class of model systems, the thickness of the oxide film and the oxide–metal interface created by growing the film are used as the decisive parameter to control the electronic structure.[107,108] This partial support system may influence either a supported deposit, as, for example, a metal atom or nanoparticle, or the film itself may be influenced by the chemical potential of the gas phase, thereby resulting in the formation of a catalytically active phase. The phenomena, observed for this second class of materials are very much influenced by the flexibility the oxide lattice of a thin film exhibits compared to the bulk material, and it may provide a new route to catalyst design.

We concentrate here on the latter case, for which we have to consider the interaction between the adsorbate on the thin film and the metal oxide support interface.[108]

To analyze the situation with the help of simple physical models one has to consider, for example, the physical quantities that determine electron transfer from the metal substrate through the film.[37] On one hand, there is the ionization potential necessary to excite an electron from the metal oxide, which is, in general, not simply the work function of the metal, because it will be substantially modified by the presence of the oxide overlayer, and, on the other hand, the electron affinity of the species adsorbed on the oxide surface, which again may be influenced by the interaction with the oxide surface. If the energy balance between those quantities results in an energy gain, then electron transfer is, in principle, possible. However, this is only part of a proper description, because it is not evident how the quantity would depend on the thickness of the film, as the energy balance will only weakly depend on it for very thin films! Of course, in the case of films with a thickness of several nanometers, the tunneling probability would simply be zero. But why would an oxide film of three layers differ from one of eight layers with respect to tunneling? The reason is connected with the increased

lattice flexibility of very thin films, which is altered very rapidly as the film gets thicker, quickly approaching the phonon behavior of the bulk or a bulk terminating surface. In other words, a thin film has the ability to accommodate the charge accumulated through electron transfer by a lattice distortion, a property that a thick film may not exhibit. This phenomenon is called polaronic distortion, and is known from metal semiconductor physics. One may use this knowledge to choose combinations of materials in thin oxide film design to produce systems with specific electronic properties in regard to electron transfer, which may in turn lead to specific chemical reactivity. Take, for example, cations, anions, or neutral species of the same species: They show different adsorption behavior and will undergo very different chemical reactions! Therefore, if we succeed in designing specific support systems that promote the formation of specific charge states, we might come to the point where we design catalysts for specific reactions. Of course, one has to consider the presence of the gas phase as well when we try to control the electron transfer by materials design, because the gas phase determines the chemical potential of a catalyst.

The examples we describe in the following address two specific questions: one concerns the charge state of metal clusters on oxide films, and the other question arises in the context of the strong metal support interaction (SMSI), when thin oxide films encapsulate nanoparticles and change their reactivity.

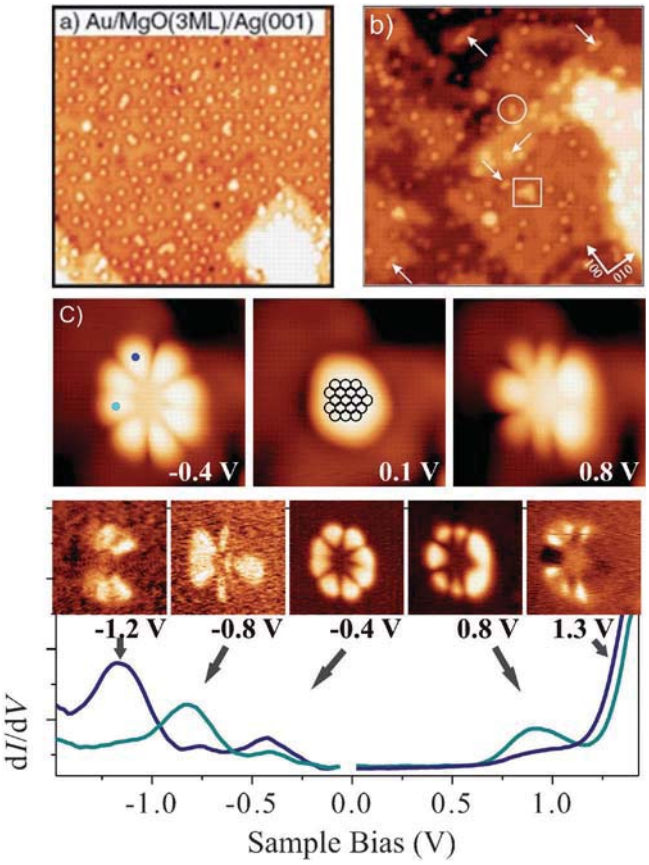

Figure 11. Scanning tunneling micrographs of a) Au atoms adsorbed on a trilayer of MgO(100) on Ag(100)[112] and b) Au clusters of varyious size and geometry on a trilayer of MgO(100)/Ag(100). Substrate direction is indicated by the Miller indices, and atoms (arrows), one-dimensional aggregates (circle), and two-dimensional aggregates (squares) are marked in the images.[112] c) Set of images of Au_{18} at three different tunneling voltages and scanning tunneling spectra of Au_{18} from -2.0 eV to $+2.0$ eV recorded at two different color-coded top positions (see image recorded at -0.4 eV). Outset conduction images have been taken for the observed maxima and the conduction bond.[113]

4.1. Au Particles on Magnesium Oxide Layers

M. Haruta[106] had already found that small gold particles, not more than 3–4 nm in size, supported on titania exhibit high catalytic activity in a number of interesting chemical reactions. Such systems catalyze CO oxidation at, or even below, room temperature, a result that is surprising, as Au is not known for its high chemical reactivity. The observations by Haruta have led to many subsequent studies with the goal of unraveling the reason for this high reactivity. Although progress has been made, the problem has not been completely resolved.[37,107,108] One open question concerns the charge state of the Au particles and its influence on the reactivity. Another question refers to the site of reaction on the Au particles. One could imagine that all the Au atoms of the particles show the same reactivity or, alternatively, some specific sites could be solely responsible for the reactivity. For example, the Au atoms at the rim or circumference of the particle, which are in contact with the oxide substrate but are still accessible from the gas phase, could be candidates for such sites. To get closer to a solution, we have prepared samples with particles of various sizes, starting from single Au atoms up to clusters containing 70 atoms or more on an MgO(100) film composed of three layers.

The oxide film was epitaxially grown on an Ag(001) surface, covering it completely, and its thickness was chosen such that electrons may be transferred from the MgO/Ag interface to the adsorbed Au particles. This charge transfer reflects itself in the distribution of the individual Au atoms on such an MgO(100) film (Figure 11 a).[109] The Au atoms try to avoid close contact because of their negative charge leading to interatomic repulsion and a wetting of the surfaces. If more Au is deposited, a variety of Au aggregates form (Figure 11 b).[110] The features shown are all atoms (arrows), one-dimensional (circles) or two-dimensional (square) flat objects. This reflects the wetting of the surface, which can be monitored as the coverage is increased, and can also be stabilized up to room temperature.[111] Had the experiments been performed on a thick MgO(100) film, the objects would have grown into three-dimensional objects instead, as typically found for the growth of metals on oxides. Clearly, thin oxide films can be used as spacers to grow ideally flat metal–insulator structures with the smallest dimensions. It is necessary to point out and remember that this statement strongly depends on the system. Had we deposited Pd instead of Au onto the MgO film, we would have observed the growth of three-dimensional objects at the end, and neutral Pd atoms with a regular diffusion limited spatial distribution at the beginning.[109,112] Therefore, the general statement found in

the literature[112] that thin films should not be used as models for bulk oxide materials is very much misleading, as it is strongly dependent on the system studied.

As stated above, clusters of various sizes were systematically studied. Au_1–Au_7 clusters, which are mainly linear, and cluster sizes between Au_{10} and Au_{20}, which are two dimensional, have been imaged.[119,114] Some examples have been studied in detail. Figure 11c shows STM images of a flat Au_{18} cluster,[120] taken at a number of different voltages. Differentiated current voltage curves (so-called scanning tunneling spectra) are plotted below the images, with the tip placed at the positions indicated by the colored dots in the images. The appearance of the images clearly depends dramatically on the imaging voltage. This is a consequence of quantum mechanics, which determines the electronic structure of the object, of course. The unpaired 6s electrons of the Au atoms constituting the cluster lead to electron wave functions of the clusters which are strongly reminiscent of an electron gas confined to a two-dimensional potential well. The potential and the number of electrons determine the nodes in the electron density. The Au_{18} cluster, according to the schematic structure shown in the inset in Figure 11c (middle), is asymmetric. If one took the Au atom at the far right side of the cluster away, one would create a symmetric Au_{17} cluster. We note in passing that, indeed, the stoichiometry of a given cluster may be established by using tip manipulation techniques.[121,115,116] To understand the electronic structure we inspected the scanning tunneling spectra, as shown in Figure 11c. The maxima correspond to the electron distribution within cluster states represented by the conduction images shown above the spectra. One may recognize the position of the nodal planes in the spatial electron distributions. The asymmetry induced by the 18th atom is also clearly visible. From the position of the nodes it is also clear why one does not observe all the maxima in all the scanning tunneling spectra: If the tip is positioned within a nodal plane no current can be detected for the specific state and consequently there is no maximum in the derivative. Tunneling spectra may be recorded for both occupied (negative voltages) and unoccupied (positive voltages) states. This allows one, in combination with model calculations and symmetry considerations, to "count" the number of electrons on the cluster.[117,120] A charge of four additional electrons is found for Au_{18}. Therefore, the proper description of the system is Au_{18}^{4-} (planar)/MgO(100).

Such considerations may be applied to any of the Au clusters of any size. Furthermore, let us consider a larger Au island containing more than 100 Au atoms, conduction images of which are shown in Figure 12a.[118] Those images may be simulated well by calculations of two-dimensional Au islands containing edges and kinks. It turns out that the charge is mainly localized at the edge and preferentially at kinks of the island. These are positions where acceptor molecules such as CO and O_2 will bind because the Au atoms are coordinatively unsaturated. Figure 12b shows experimental evidence for this: On the left, a topographic STM image of a randomly chosen island that was exposed to CO is shown, and on the right the same island is imaged in a mode (second derivative) that allows for detection of inelastic losses in the tunneling current.[126] In this particular case, the characteristic frustrated

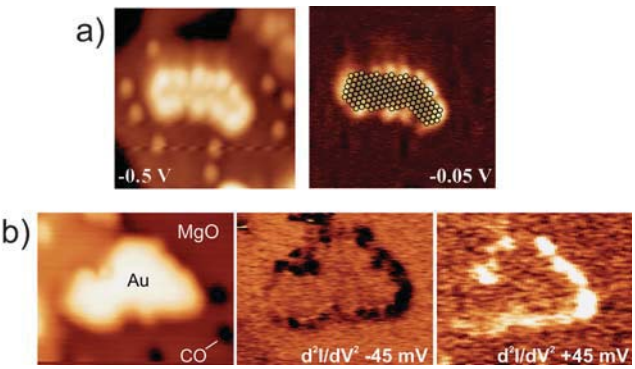

Figure 12. Scanning tunneling micrographs[125] of larger Au islands supported on a trilayer of MgO(100)/Ag(100): a) Image taken at $U_s = 0.5$ eV and b) a conduction image emphasizing the edge states. A schematic atomic model of the island is overlayed. c) STM image of an arbitrary island after exposure to CO (left). Inelastic tunneling images of the same island recorded at the energy of the frustrated CO rotor frequency for loss and gain (45 meV; middle and right).[119]

rotation of adsorbed carbon monoxide at 45 meV excitation energy has been probed and used for imaging. Vibration is found in these images both as a gain (bright) and loss (dark; processes that may both happen during inelastic tunneling) only at the rim of the island, thus illustrating and identifying the preferential adsorption sites of CO molecules. when it comes to CO oxidation, one may, therefore, consider a scenario where both CO and O_2 bind to the cluster rim, and O_2 reacts either directly or after dissociation with coadsorbed CO to afford carbon dioxide. With this example we leave the world of supported metal clusters and we turn to the reactivity of thin oxide films themselves.

4.2. CO Oxidation on a Highly Reactive FeO(111) Film Supported on Pt(111)

Strong metal support interaction (SMSI) is observed for particular catalyst systems, in which metal particles (such as Pd and Pt) strongly interact with a reducible support (such as titania) and are covered by a thin oxide film upon heating to an elevated temperature.[120,121,125] Such systems usually show reduced catalytic activity. The oxide film leads to a strong attenuation of adsorption capacity and, consequently, to a deactivation of the system. There have been many attempts to elucidate, even with model systems, the nature of the migrating oxide film. The best studied system is Pd/TiO_2, but even in this case attempts to identify the exact nature of the oxide have not been successful.[122,123] Very recently, we succeeded in preparing such a SMSI model system, in which we are able to identify the nature of the migrating oxide. The system is Pt on $Fe_3O_4(111)$ grown on a Pt(111) single crystal.[124,125]

Figure 13 shows an STM image of this system after heating it to 850 K. The CO adsorption capacity is drastically reduced after this treatment, which is typical for a SMSI effect.[127,128] A close look at the STM images reveals well-structured and facetted nanoparticles. Moreover, atomically

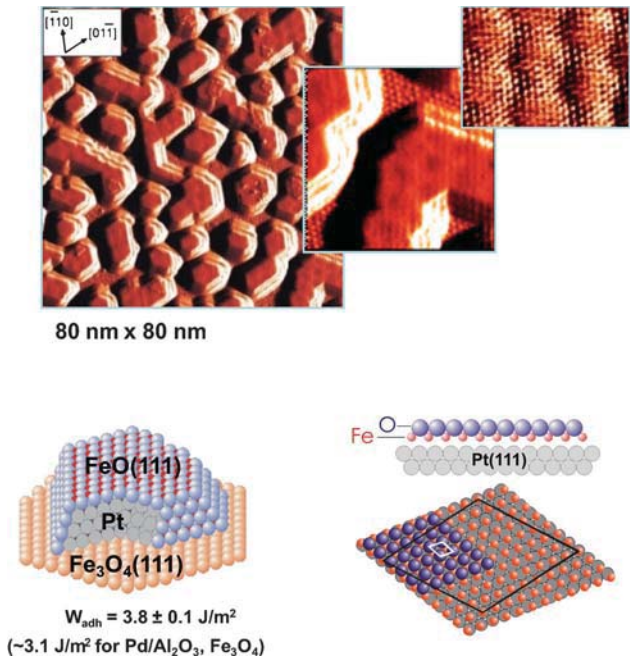

Figure 13. Scanning tunneling images of Pt nanoparticles supported on a Fe_3O_4(111) film grown on Pt(111) (the magnetite film thickness represents the bulk) after heating to 850 K.[131,132] Schematic representation of the formed FeO-encapsulated Pt nanoparticles together with the mark of adhesion determined by a Wulff–Kaichev analysis compared to those determined in the same way for Pd supported on different substrates.[132,138] Schematic representation of the double-layer FeO film grown on Pt(111) together with the determined structural parameters.[134,135]

resolved images reveal corrugation that does not stem from Pt but rather from a well-ordered double-layer FeO film, which has been well-described and characterized in the literature.[126–129] A schematic representation of the situation is depicted in Figure 13b, and the work of adhesion of Pt on Fe_3O_4 is given.[127c] A comparison with Pd on different substrates indicates that Pt is more strongly bound than Pd on the same substrate.[130,132] This increased work of adhesion is likely to be responsible for the occurrence of the SMSI phenomenon. As the oxide film has been identified, one may reduce the complexity of the model system by studying the properties of the bilayer FeO film on a Pt(111) single crystal. Its structure has been studied in detail and characterized at the atomic level.[134–136] The large misfit between the FeO lattice constant and that of Pt(111) results in a large unit cell, which gives rise to a typical Moiré pattern in the STM image. This film is unreactive under ultrahigh vacuum conditions.[131] The situation changes, dramatically, however if one tests the system with respect to CO oxidation at ambient conditions (1 atm) in a reactor[131] with careful control of the relative amounts of oxygen (one part, 20 mbar), carbon monoxide (two parts, 40 mbar), and helium as buffer gas. Increasing the temperature linearly at 1 K per minute from 300 K to 455 K shows that CO oxidation starts at 430 K.

The interesting observation is that this FeO/Pt(111) system is more than an order of magnitude more reactive than clean platinum at this temperature. Usually, SMSI leads to an attenuated activity, while here we observe a strong enhancement! Other similar studies with different gas compositions, as well as thermal desorption studies, scanning tunneling microscopy investigations, and detailed density functional model calculations reveal an interesting scenario that allows us to understand this phenomenon.[131]

The scenario is depicted in Figure 14a. The gas phase sets the chemical potential of the system. The shown steps are based on density functional calculations. Oxygen interacts

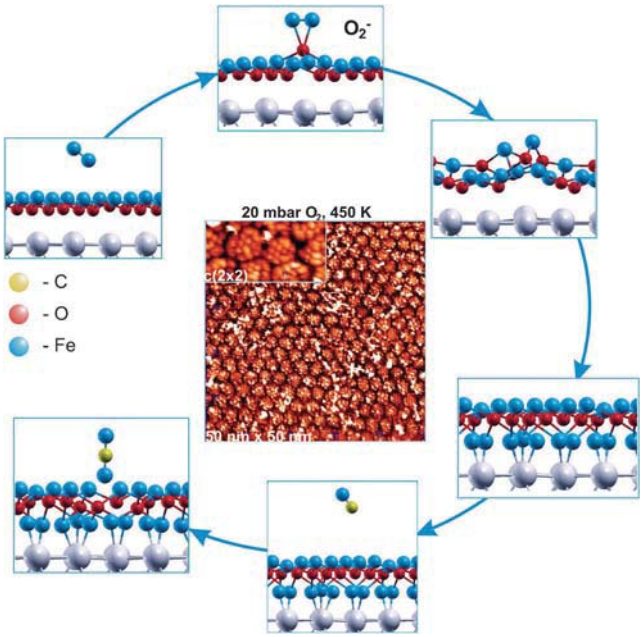

Figure 14. Schematic representation of results of DFT calculations performed by Pacchioni, Noguera, et al. which simulate the elementary steps in the interaction of FeO/Pt(111) with oxygen to form a reactive intermediate FeO_{2-x} trilayer and the subsequent oxidation of CO to CO_2 in this layer by a Eley–Rideal–Mars–van-Krevelen mechanism.[131] An experimental scanning tunneling micrograph of the in situ prepared reactive FeO trilayer is shown in the middle.[131]

with the double-layer FeO film on Pt(111) by pulling an iron atom up above the oxygen layer. This lowers the work function at the interface locally to allow for an electron transfer towards oxygen accompanied by the formation of a transient O_2^- molecule, which dissociates and results at higher oxygen coverage in the formation of a local O-FeO trilayer. There is, indeed, experimental evidence for the existence of such a trilayer. The middle panel in Figure 14 shows an STM image of such a trilayer formed in situ at elevated O_2 pressure in a microscope.[131,134] Its appearance is in particular determined by the Moiré structure of the FeO double layer and fills 80–90% of the surface, as thermal desorption spectra indicate. The images are completely consistent with the structure suggested by the calculation, although the latter does not reproduce the patched morphology because of the enormous size of the unit cell, which was impossible to implement, but necessary to fully reproduce the details. Nevertheless, if the trilayer is exposed to carbon monoxide it oxidizes the incoming CO to form CO_2 by an Eley–Rideal

mechanism, thereby leaving behind an oxygen vacancy in the film. If the oxygen pressure is sufficiently high, the oxygen vacancy is filled again and the trilayer is sustained. If, however, the gas phase is oxygen-poor the reaction finally stops because the trilayer is destroyed. We have confirmed experimentally[131] that the iron oxide film de-wets the Pt(111) surface under oxygen-rich reaction conditions by forming small iron oxide particles, thereby leaving the underlying Pt(111) surface open, which determines the reactivity of the systems. Heating the de-wetted surface in oxygen again leads to the formation of the FeO double layer, which then, at higher oxygen pressure, may be transformed into the trilayer again.

In summary, we are in a position to understand the phenomena in this case on a similar basis as the first examples on supported small metal clusters, as the electron transfer to oxygen is the key step to initiate the process. Superficially, we may come to the conclusion that we have identified a new concept to look at catalytic systems. Closer inspection reveals that this concept was used in the late 1940s by Cabrera and Mott[132] to understand metal oxidation and in the 1950s and 1960s by F. Vol′kenshtein to explain catalytic activity.[133] A quote from one of his papers from 1966 supports this:[7] "*…the semiconductor* (oxide) *film arises as a result of oxidation of a metal, and its thickness can often be controlled to some extent…By varying the thickness..it is possible to…control…the adsorption capacity, the catalytic activity, and the selectivity… It would be interesting to study the adsorption and catalytic properties of a semiconducting film on a metal, and their changes, during growth of the film*". This concept was revived in the late 1980 is by Frost[134] and subsequently discussed by Boudart[135] and Ponec.[136] It was eventually forgotten and not followed up, probably because tools to study such systems systematically at the atomic level were not yet available. The time has now come!

Clearly, thin oxide films on metal substrates represent an interesting and promising combination of materials. It is possible to use well-known concepts from semiconductor physics to understand the underlying principles and to use them to design model systems to get insight into elementary questions in catalysis. In both examples discussed, electron transfer determines the reactivity. It is quite possible to think about materials combinations which would favor electron transfer for specific molecules and induce specific and selective reactions. Maybe these new (old) concepts could be used as a guideline to design catalysts. It should be noted that it is crucial to have the appropriate experimental techniques at hand. The design of a useful set of experimental techniques is a key goal of experimental research.

5. CO Oxidation as a Probe Reaction in Industrial Catalysis.

High-performance catalysts with complex structures present an analytical challenge when it comes to determining the number of active sites per unit surface area. Knowledge of this quantity is a prerequisite for quantifying "catalytic activity". The concept of turnover frequencies enables catalysts of very different kinds to be compared in one and the same reaction provided that we know the number of active sites per unit weight or unit surface area. It is, however, very difficult to determine the number of active sites on a real catalyst. One way of obtaining this number is the use of a probe reaction that occurs with well-known kinetics at active sites that are identical or chemically similar to those of the reaction of interest, but exhibits a more complex kinetic pattern. CO oxidation should be a suitable probe reaction for catalytic redox reactions (hydrogenations, oxidations). This reaction is a redox reaction, it operates in a "simple" Langmuir–Hinshelwood mode and can be quantified easily—as its sole product is CO_2, which desorbs easily from many catalyst surfaces of relevance, with some notable exceptions.[7]

We know for certain from surface science[18,21] that CO oxidation may proceed without materials gaps over single-crystal model surfaces as well as over high-performance catalysts. For the case of Pd this was verified in two sets of rigorous molecular beam studies on single crystals[4] and on supported nanoparticles.[6] Different catalysts were compared by their conversion of CO to determine the identity of the active sites through their apparent activation energies and for their number of active sites. In this way, many extrinsic test variables are normalized out, provided that the tests are conducted without macroscopic transport limitations. The comparison of single-crystalline palladium and palladium nanoparticles yielded a common reference value for the activation energy for CO oxidation over Pd metal of 135 $kJ\,mol^{-1}$.

It is, however, inappropriate to deduce any mechanistic information from such numbers, as the activation energy is related to elementary steps through a network of adsorption, surface diffusion, and reactions. This has been outlined in the molecular beam studies,[4] which have lead to a generic criticism of over-interpretation of macrokinetic observables in terms of "mechanism". In later studies a range of observable activation barriers between 58 $kJ\,mol^{-1}$ and 146 $kJ\,mol^{-1}$ was deduced from several boundary cases of adsorption and reaction on Pd(111). This means that any value between these boundaries can belong to CO oxidation over Pd metal. The only difference may be the surface structure controlling the oxidation mechanism under identical test conditions. Surface dynamics[12a] that lead in fortunate cases to strong coupling with the oscillatory behavior can occur whenever boundary cases of surface structures coexist with small energetic differences in the thermodynamically open system.[29] Probe reactions should, thus, not be over-interpreted: as a consequence of the cooperation of several elementary steps in the probe reaction, they sense multiple properties of surfaces that may vary within a set of samples.

With these limitations in mind we can still use CO oxidation as a probe to find sites on a catalyst that allow for the coexistence of chemisorbed CO and atomic electrophilic oxygen. The site must, thus, consist of an ensemble of atoms that allow for an electron-accepting Lewis function to adsorb CO and for the stabilization of an electron-poor form of atomic oxygen (weakly bound) that is capable of oxidizing CO. Good catalysts for CO oxidation are found in the

Periodic Table where the ability for electron back-donation to CO is limited and the redox potential is "noble" enough not to form strong metal–oxo bonds. This is apparently the case with the Group VIII metals, where we indeed find highly potent catalysts for CO oxidation.

The following examples of oxide and metal catalysts will show that different realizations of such sites can exist with chemical compounds. We thus have to add a "materials caveat" to the kinetic caveat mentioned above: it should not be attempted to conclude the chemical nature of the active sites when analyzing the results of CO oxidation probe reactions. Despite these limitations towards the atomistic interpretation of probe reaction data, it is useful to perform such experiments to find a meaningful way of comparing the performances of catalysts. The method can further discriminate the electronic state of adsorbed oxygen when the same catalyst is probed for CO oxidation and for another reaction which is differently selective for the electronic nature of the active oxygen,[137] such as alcohol oxidation.

The first example concerns the oxidation of propane to acrylic acid over the complex oxide $MoVNbTeO_{4-x}$ (M1 phase).[138] The reaction proceeds through a complex network of processes involving both the action of nucleophilic oxygen for C–H activation and of electrophilic oxygen for the addition of oxygen to the hydrocarbon.

$$C_3H_8 + 2\,[O_{nucleo}] + 2\,[O_{electro}] \rightarrow C_3H_3OOH + 2\,H_2O \quad (7)$$

CO and CO_2 are formed as by-products, thus indicating that there is either a shortage of electrophilic oxygen in the system or there are no adsorption sites for CO—which is quite possible on an oxide with on average high oxidation states held at 673 K. Kinetic experiments at ambient pressure with well-activated catalysts were carried out by feeding CO instead of propane into the system. Figure 15 shows the results for two different catalyst preparations with the same M1 phase. The consumption rate propane is two orders of magnitude higher than that of CO, with both measured at the same chemical potential of oxygen. The likely blocking of the sites by water molecules is not responsible for the poor CO oxidation activity, as the addition of 40% steam only slightly enhances the reaction rate.

Propane activation requires only nucleophilic oxygen.[139] In the course of this reaction, defects and hence Lewis sites are created, where electrophilic oxygen may be adsorbed. The enormous rate difference for CO oxidation thus allows the conclusion to be drawn that the sites required for CO oxidation are not part of the genuine catalyst structure, as it seems that electrophilic oxygen is not adsorbed at these sites. Electrophilic oxygen may only form as a consequence of a prior activation of propane. Adsorption of CO will only occur on metal sites with low oxidation states, which do not exist on M1 in the presence of oxygen, which in turn are necessary to activate propane and create the sites for electrophilc oxygen. The dynamic situation of reactants controlling the surface state of the catalyst is clear. This explains the unexpected result of the very poor reactivity of M1 towards CO, a system that can oxidize the non-activated propane molecule. The probe reaction experiment further confirms that CO oxidation also occurs through a Langmuir–Hinshelwood mechanism[4] under the conditions of alkane oxidation. An Eley–Rideal mechanism of CO oxidation would involve electrophilic oxygen, but would not require low-valent adsorption sites that cannot coexist with activated oxygen on an oxide surface, and thus would proceed with a high rate.

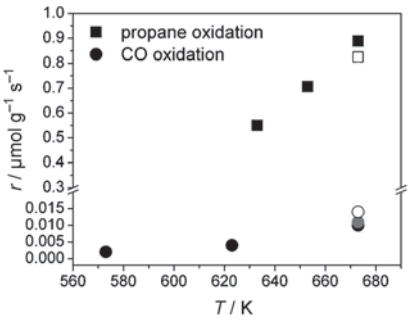

Figure 15. Rates of consumption of propane and CO over a polycrystalline complex oxide catalyst ($MoVNbTeO_{4-x}$; M1 phase). The molar ratio of the reactants in the feed for the oxidation of propane corresponds to $C_3H_8/O_2/H_2O/N_2 = 3:6:40:51$ vol%. The measurements were performed at a contact time of 0.81 g(cat.) s mL^{-1} (filled squares). A different M1 batch was measured only at 673 K and a contact time of 0.80 g(cat.) s mL^{-1} (open square). CO oxidation was performed using the latter batch at a contact time of 1.2 g(cat.) s mL^{-1} in dry feed composed of $CO/O_2/H_2O/N_2 = 3:6:0:91$ vol% (black circles). Decreasing the contact time to 0.80 g(cat.) s mL^{-1} at 673 K results in only slightly increased rate of CO consumption in the dry feed (gray circle) and in the presence of 40 vol% steam ($CO/O_2/H_2O/N_2 = 3:6:40:51$, open circle).

A prominent example of CO oxidation over an oxide surface is the case of RuO_2. Thorough studies[140] of the action of atomic oxygen on Ru metal resulted in the discovery of a complex sequence of events ranging from adsorption through formation of subsurface compounds[141] to bulk oxidation. Precise determination of the structure of the UHV termination of a thin film of RuO_2[34,142] led to reaction studies that culminated in the "unmistakable" identification[19] of that phase as the most active catalyst for CO oxidation; however, only under relatively mild reaction conditions. This view, although initially confirmed experimentally, is strongly opposed by experiments under more drastic (higher pressure) conditions,[17] which concluded that an oxygen chemisorption phase and not the oxide would be the most active phase. The vigorous debate on this issue led to the hypothesis that both views may be correct under their respective set of conditions; the interaction of atomic oxygen under the moderating influence of CO may lead to a series of chemically different states for Ru. An adsorbate phase will gradually populate the subsurface regime of the metal at increasing chemical potential, thereby leading to disordered surfaces[152] and finally to the formation of a thin film[143] of ordered RuO_2. This was confirmed experimentally by ambient-pressure photoemission[144] and photoelectron microscopy.[22] The most active phase for CO oxidation was found to be the oxygen-rich subsurface phase, which tends to coexist with patches of the RuO_2 phase. Thus, no effect on the CO oxidation rate is detected when crossing the phase boundary[152] between the RuO_2 and subsurface oxide phases.

Exactly the same behavior was also found for the selective oxidation of methanol,[145] where the transient surface oxide (TSO) was the most active state, irrespective of whether starting from the pure oxide or from metal phases.

CO oxidation as a probe reaction on high-performance nanoparticle Ru catalysts was used to identify[146] a highly active state of patchy particles, possibly similar to the TSO state, and a state of lower activity that consists of a thin closed film of RuO_2. It was clearly established that the composition of the reactant gas phase critically controlled the activity: this is not due to modifications of the adsorbate phase as discussed[4] with Pd at low pressure, but occurs as a dimension of the chemical dynamics of the Ru phase. The plasticity of RuO_2, which can tolerate the coexistence of two phases[147] with different oxidation states, was also confirmed to exist on the mesoscale by using micrometer-sized single crystals of phase-pure RuO_2. These crystals shown in Figure 16A are inactive in CO oxidation as long as they are not reduced to the TSO state at their surface. It was found to be possible[148] to retain the bulk oxide structure during CO oxidation at ambient pressure, as seen by in situ X-ray diffraction, and identify simultaneously (Figure 16B) reduction of the crystal surface of certain facets to a textured (Figure 16C) metallic state.

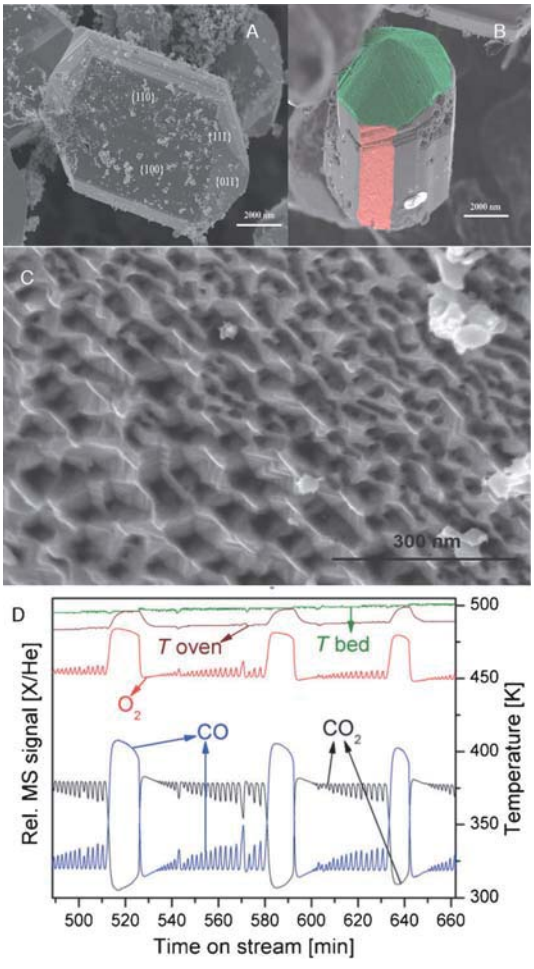

Figure 16. Dynamic behavior of stoichiometric RuO_2. For details see Ref. [161]. A) A defect-poor crystal of RuO_2 with surface orientations determined by EBSD. B) After CO oxidation some faces (colored) are roughened. C) Microstructure of the roughened surfaces exhibiting a large excess of Ru over O as determined locally by EDX. D) Rate oscillations during CO oxidation in in situ XRD, which reveal bulk RuO_2 as the support phase.

The analysis of activated RuO_2 (as verified[152] by in situ XRD) reveals the formation of richly structured Ru-rich surface films on certain facets, whereas other orientations stay completely unaffected by the presence of even a large excess of reducing CO. The redox plasticity can also give rise to kinetic oscillations in CO oxidation at ambient pressure. Figure 16D shows an example where two processes of different time scales are interconnected. One process that completely shuts off the activity of the catalyst is related to a strong exothermic reaction associated with full oxidation of the catalyst to the deactivated form RuO_2. The active form is a partly reduced state, probably as depicted in Figure 16C. The other process gives rise to fast oscillations that modulate the performance. The sensitivity of the temporal evolution to the gas phase potential and the local heat transport leads us to assign this fast process to surface dynamics possibly associated with changes in the local coverage of CO and the oxygen content of the TSO state. These dynamics, being in analogy to the surface dynamics discussed for Pd, is also thought to generate the fine structure seen on the facets in Figure 16C.

The application of CO oxidation as a probe reaction with Ru catalysts has brought about a whole range of insights into the complexity of metal-oxide transitions and their role in catalytic oxidation. Summarizing the ambient pressure results and comparing them to those of the model studies of surface analysis mentioned above allows the following picture to be deduced.[162] As the oxidizing potential (given by partial pressures at the surface, sticking coefficients, and heat flux) increases, the bare metal is first covered by an adsorbate layer. At higher potentials the surface oxygen goes under the surface and forms a solid solution and eventually the TSO state (approximated by the so-called[29] trilayer model). In this state the surface is nanostructured and rough. From there patches of the dioxide evolve, eventually growing with substantial kinetic hindrance into a dense film. The most active state seems to be the state where the TSO is rich in oxygen and begins to order into the dioxide. The inverse process, which occurs with quite different kinetics, involves a structure-sensitive partial reduction of a stoichiometric amount of a dioxide into a mixed state of a film of TSO that coexists with oxide facets. Only under drastic conditions of reduction potential and local overheating (for this reason, high concentrations of CO are not activating at typical operation temperatures) is the dioxide converted in a nucleation-controlled reaction into an agglomeration of metal nanoparticles with ample grain boundaries that contain TSO states.

This picture of redox plasticity is in good agreement with theoretical studies of the system. It was found by combining ab inito treatment of the system with surface thermodynamics and with statistical mechanics[149] that the most active state of the reacting surface occurs at the boundaries of stable adsorbate phases, where multiple states can coexist[150] at similar energies. It was further found[29] that the intuitively

assumed reaction of adsorbed CO with terminating oxygen (cus sites) is not the most active reaction path but rather a coadsorption process of CO and predissociated oxygen at bridging metal sites. This may be seen in regard to the activity of the TSO state, which also contains metal sites with local electronic structure modified by neighboring oxygen species that are, however, more weakly bound[151] than cus oxygen species.

Both the TSO phase and the "Ertl/Over oxide" (see Figure 21) are thin heterostructures. Their effect as collective moderators of the electronic structure of adsorption sites for CO and oxygen may be as important as the local electronic effect of d-band bending on mixing oxygen atoms with Ru atoms. Even if the net effect of moderating the adsorption enthalpies is the same, the consequences for designing and optimizing catalysts would be different if thin two-dimensional overlayers, as they also are described in Section 4 of this Review, are suitable tools for tuning surface adsorption properties.

We now return to the case of Pd in CO oxidation. We describe here experiments in which the reaction is different for Pd nanoparticles supported on carbon nanotubes (CNT)—which are useful catalysts for synthesis of H_2O_2[152]—and Pd nanoparticles supported on iron oxides. The latter system is studied as the redox chemistry of iron oxides allows for different types of metal–support interactions within nanoparticles that are accessible in a homogeneous form through co-precipitation with the support. The Pt/iron oxide system was investigated[127c,153] with model systems, and a strong effect of the metal–support interactions was found for CO oxidation. In the case of the analogous Pd/iron oxide system, the unexpected reduction in the heat of adsorption of CO with decreasing particle size was detected,[154] thus allowing speculation that small particles may be more active in CO oxidation because the strong site blocking of adsorbed CO may be reduced.

A series of iron oxides based upon hematite (Fe_2O_3) with a surface area of 27 $m^2 g^{-1}$ was prepared by co-precipitating 2% Pd into the system. The surface area increased to 163 $m^2 g^{-1}$ after mild reduction (673 K), whereas the surface area was only 47 $m^2 g^{-1}$ after harsh reduction (823 K). Reduction of the Pd led to reduction of hematite to magnetite (Fe_3O_4), which could be reoxidized to maghemite (γ-Fe_2O_3). It was shown by in situ XRD that the properties of the catalysts did not depend upon the bulk iron oxide phase, similar to the case of ruthenium oxide.

Two types of Pd particles were found: a minority of three-dimensional particles of about 4–6 nm size, which exposed the (111) face, and the vast majority of particles of about 1.5 nm diameter that were not detectable by high-resolution electron microscopy (HR-TEM). These particles are raftlike, as a spherical morphology would have been detected by HR-TEM. Substantial effort was taken to synthesize reproducibly such small particles so that they were comparable with those reported in the literature.[112] A significant depression of the CO adsorption energy (110 kJ mol^{-1}) is expected with respect to the value[4] for a single-crystal surface, thereby leading to a better reactivity. Mild reduction allowed, unexpectedly and only for co-precipitated systems, the synthesis of an SMSI state[155] in which the Pd is overgrown by iron oxide as seen by in situ XPS and by TEM in Figure 17.

The in situ XPS experiment at ambient pressure verified that the overgrowth is destroyed upon reduction of the iron oxide. Reoxidation of the system occurred easily without, however, restoring the SMSI state. This state occurs only upon initial activation of the catalyst. Chemical reduction destroys the overlayer oxide, but seemingly also alters the metal support interaction, as the overlayer was not restored under the conditions applied. The aberration-corrected bright-field TEM shows a real-space image of such an overlayer structure. The image gives a good impression of the relative sizes of the support and active particle. It further reveals that the overlayer occurs on all the edges of the support and that it is not a special structure that occurs only at

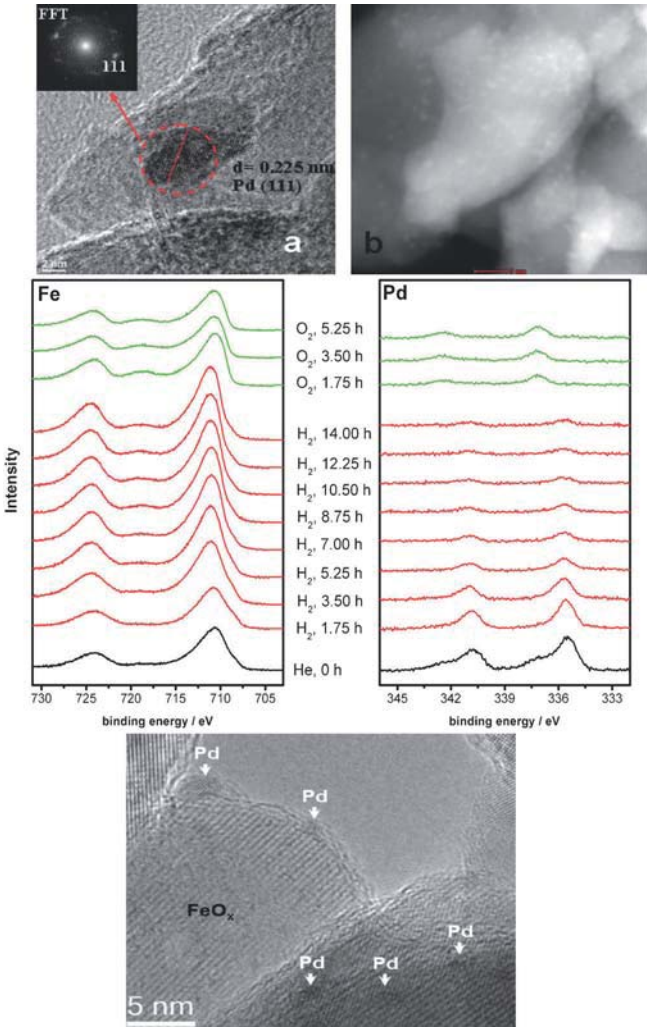

Figure 17. Pd nanoparticles on iron oxides. a,b) HR-TEM and STEM-HAADF images of Pd particles. Only a few large Pd particles are visible in the HR-TEM image, which is typical for many catalyst systems. Only with HAADF is it possible to identify the majority species. The in situ XPS experiment documents the loss of free Pd upon reduction (red traces, the long reaction time is needed as the experimental pressure is only 1 mbar). Reoxidation (green traces) increases the free Pd surface in the form of the oxide. The bottom aberration-corrected HR-TEM image indicates the existence of an overlayer on the Pd nanoparticles. From XPS we can exclude carbon as the origin.

the Pd particles. Thus, a redox reaction of the support will destroy the delicate overlayer and that it will not reappear once its material is built into the crystals of the iron oxide.

The kinetic response of Pd/hematite in the SMSI state is shown in Figure 18A. The initial stable apparent activation energy of 33 kJ mol^{-1} is low and outside the range of expected values for pure Pd, as deduced from mechanistic considerations discussed above. Cooling from 473 K back to 300 K and repeating the experiment leads to deactivation not only by sintering (this would give rise to a parallel line in Figure 18A) but also by partial loss of the SMSI state with creation of new but less-active sites. This process continues under harsher reaction conditions, with the activation energy changing from 46 kJ mol^{-1} over 53 kJ mol^{-1} to 70 kJ mol^{-1}, which is now well within the expected range. The experiment shown in Figure 18A requires several days of continuous experimentation and clearly reveals the structural dynamics of the system. As none of these changes were reversible it is assumed that we observe both sintering and delamination of the SMSI state simultaneously. In Figure 18B the TEM-HAADF (high-angle annular dark filed detector) image of a used sample indeed reveals some sintering that is, however, moderate with respect to typical aggregation effects[156] of Pd. The contrast within the support shows the creation of defects (protrusions) following the bulk redox reactions of the support upon changing the chemical potential of the gas phase. This bulk response occurs from in situ XRD observations being fast compared to the kinetic responses and is thus a dynamic event decoupled from the surface chemistry sensed by the CO oxidation probe reaction.

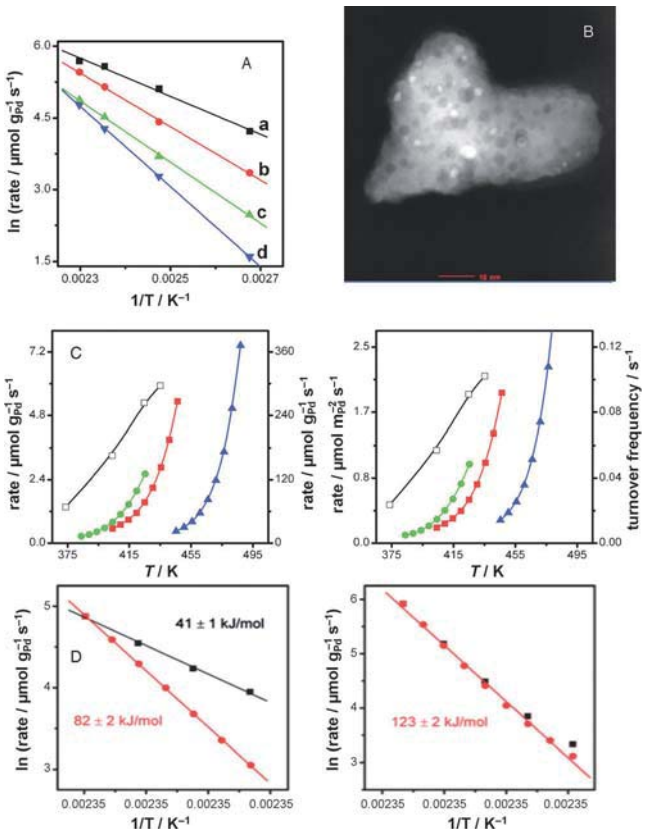

Figure 18. Performance of nano-Pd in CO oxidation: A) Steady-state activation energy measurements of Pd on hematite (a fresh, b after cooling to RT, c after oxygen-rich feed, d after cooling to RT). B) HAADF-STEM of a sample after treatment (a) in (A). C) CO conversion rates with several normalizations as a function of temperature at 25% constant conversion and after long-term (300 h) stabilization: filled squares: Pd/H after reduction at room temperature; circles: Pd/maghemite after reduction at 523 K; triangles: Pd/CNT after reduction at 523 K; rates are normalized to sample mass, to Pd sample mass (using a Pd content of 2.0 wt% for all samples), to specific Pd surface area derived from CO chemisorption experiments, and to the number of Pd surface atoms (turnover frequency), assuming that every Pd surface atom represents an active site. Data were measured with Pd/H in the SMSI state, directly after reduction at 523 K without deactivation test, is included for comparison (hollow squares). D) activation energies of long-term stabilized Pd/maghemite (523 K) and Pd/CNT: black during heating the sample and red during cooling.

The rates of CO oxidation of several systems are compared in Figure 18C. The SMSI state is clearly superior to the performance of the other systems. Compared to those on the nonreducible carbon support, the Pd nanoparticles on iron oxide are still superior despite the same size distribution on all the catalysts (90% between 1.5 and 2 nm). The shape of the curve representing the temperature dependence of the oxidation rate is different for the SMSI state and for all the other states, thus indicating that different surface kinetic conditions are dominating; in the SMSI state and at high temperatures the catalyst seems free of blocking CO, which strongly reduces the activity of bare Pd at lower temperatures. The experiments, which give quite different absolute values for the "catalytic activity" in different normalizations, are fully reproducible as long-term conditioning (60 h) was applied prior to data acquisition.

The results illustrate the difficulties in how to define the number of active sites. The ability to quantify them by using CO oxidation is, however, clearly demonstrated. It is clear that data reduction to intrinsic active site numbers would require microkinetic modeling; in view of the multiple surface and chemical dynamic effects congested into the one observable, this endeavor is difficult, even for such a simple reaction as the oxidation of CO.

The equilibrated systems allow the stable apparent activation energy for CO oxidation to be determined. In Figure 18D it is seen that Pd/CNT shows the expected behavior (123 kJ mol^{-1}) during temperature cycling, thus indicating that the various surface states of reactant blocking interconvert[4] with no detectable effect in these macrokinetic experiments. Pd supported on hematite reveals an apparent activation energy of 82 kJ mol^{-1}, with, however, a significantly higher rate during heating than cooling. This implies some reversible loss of sites through either sintering and redispersion or deposition and oxidation of carbon at high temperatures. Both processes could be reversible below 500 K. Pd on maghemite shows, however, the unexpected strong deviation from a universal Arrhenius behavior (Figure 18D. Its activation barrier upon heating is 42 kJ mol^{-1}, which is only half that during cooling, where the normal value for these systems is attained. As these experiments were all conducted over long times at steady state it is clear that several mechanisms of dynamic behavior operate in the Pd/iron oxide system. CO oxidation is a suitable probe for

detecting these phenomena, but it is unsuitable to explain their origin. The interplay between SMSI and particle coalescence is one element of dynamics, but the partial reversibility upon changing the chemical potential is unexpected under these mild reaction conditions. The dynamics is independent from bulk transformations of the support, which according to in situ XRD measurements occur on a faster time scale of several hours.

In conclusion, CO oxidation is a sensitive tool for probing the redox reactivity of polycrystalline and nanostructured catalysts both in the oxidic and in the metallic states. It is desirable to relate probe reaction experiments on CO oxidation to model studies with known structural and dynamical behavior and to theoretical reaction studies (as illustrated in Sections 4 and 6) when analyzing high-performance systems. The SMSI state on Pd nanoparticles was unexpected, with its search being motivated by similar observations with Pt model systems. The oxidation of CO can be used to discover the dynamics of high-performing catalyst systems that arise from the coupling of the surface chemistry to the gas-phase chemical potential. The examples have shown that quantitative analysis is probably still premature, but that a fingerprint comparison of the reactivity of various systems can be achieved with high "chemical resolution" of different active states. Such data may be compared to theoretical descriptions of complex catalysts. This can give insight into the detailed nature of the active sites, which is still not accessible experimentally, as they always represent minority species on reactive surfaces. The method of measuring CO oxidation kinetics in combination with in situ structural analysis deals with the possibility of material gaps remaining undetected by static analysis. The application of the CO oxidation probe reaction technique can thus give answers about the abundance and dynamics of active sites on high-performance catalysts, where spectroscopic and surface analytical techniques only give average information about the reactive and adsorptive sites. This is possible as we can interpret the quantitative results of CO oxidation on the basis of a conceptual understanding of the reaction.

6. Get Real! CO Oxidation at Realistic Temperature and Pressure

This section focuses on ab initio (from the electronic structure) multiscale modeling[157] of CO oxidation at realistic (T, p) conditions and a description of the steady state of catalysis. A key finding is that the composition and structure of the catalytically active material are very different under reactive conditions, that is, in the open thermodynamic environment of the ongoing surface chemical reactions, than at low pressure or thermal equilibrium. In principle, such changes in the material are well known and, for example, are reflected in the observation that the performance of a catalyst typically develops over a macroscopic induction period. Despite the crucial significance of these changes for the electronic and reaction properties, an atomistic/microscopic understanding is essentially lacking. Experimentally this is due to the fact that experiments with atomic resolution are difficult or (so far) impossible to do under the (T, p) conditions of catalysis.[20,158–162] Theoretically, the difficulty is related to the lack of reliable information about the surface structure and composition and/or the involved time scales. The latter may be in the range of milliseconds or even hours.

CO oxidation is a strongly exothermal process. In the gas phase the reaction is spin forbidden, because the reactants have total spin $S = 1$ (because of the triplet ground state of O_2) but the reaction product (CO_2) has zero spin. However, for dissociated O_2, where the individually adsorbed O atoms are in a spin-zero state, the reaction can proceed. It may be slowed down by an energy barrier though, and to understand its magnitude and relevance we need to know and consider at what material the reactants will adsorb. Clearly, it is also necessary that the adsorbed CO and adsorbed O occupy nearby positions and to take into account the appropriate statistical average over space and time to determine the turnover frequency (TOF), that is, the number of CO_2 molecules formed per square centimeter of the catalyst's surface area per second.

The predictive modeling of heterogeneous catalysis must address the steady state of the operation. As we will discuss below, the statistical mechanics of the interfering dynamics of various atomistic processes reveal the significance of instabilities and fluctuations: A catalyst is a "living" object that is subject to incessant changes even in its steady state. In fact, we stress that these instabilities and fluctuations are crucial for a self-healing of locally poisoned regions and therefore for the long-term operational stability of the catalyst. They are in particular present and relevant under conditions of high performance and may be absent under other conditions.

Figure 19 outlines the theoretical challenge. The base of predictive modeling must be a reliable description of the electronic structure regime that accounts for the bond breaking and bond making at the catalyst surface. Such a theoretical description must, however, be linked to statistical

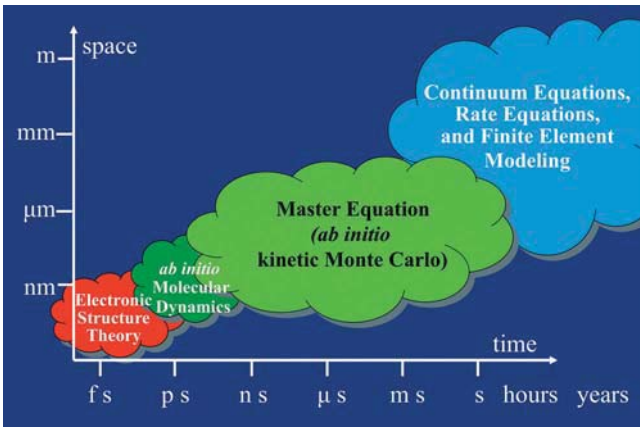

Figure 19. Time and space scales relevant for materials science application, as, for example, heterogeneous catalysis. The elementary processes of bond breaking and bond making between atoms and molecules are described by "electronic-structure theory". This is the base for everything that follows. The interplay of many molecular processes then determines the function of the catalyst that only develops over meso- or macroscopic lengths and times.

mechanics because under realistic environmental conditions the surface of the material may change significantly and possibly even deeper (see the discussion on the "induction period" above). The steady state of catalysis results from appropriate time and space averages of the statistical mechanics, and we will see that a "one-structure, one-site, one-mechanism" description is typically not appropriate for a thorough understanding.

It is well known that metals will change when exposed to a realistic atmosphere. For example, iron will rust. Even though such changes may be thermodynamically favorable, they may still be slow and confined to the surface region. For example, the corrosion of metals stops after some nanometers because the low rate of dissociation of O_2 or diffusion of O or metal atoms prevents thermodynamic equilibrium from being reached on human time scales. If the atmosphere contains CO, the oxidation of the metal may be reversed because of the reducing activity of CO arising from the low energy of CO_2. Although catalysis is clearly not a thermal equilibrium process (the detailed discussion follows below), it is nevertheless useful to consider which thermal equilibrium structures may be close.

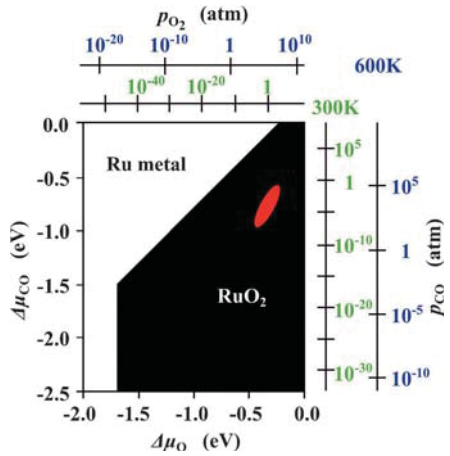

Figure 20. Calculated phase diagram of Ru in an O_2 + CO atmosphere. The left and bottom axes give the chemical potentials that enter the calculations. The top and right axes give the corresponding pressures at two different temperatures: $T = 300$ K and $T = 600$ K. For details see Ref. [163]. The region where catalysis operates is indicated by the red area.

Figure 20 shows as an example the phase diagram of Ru when held in an atmosphere of O_2 and CO. Strictly speaking, this is a so-called constrained thermal equilibrium because the gas-phase reaction of CO and O_2 towards CO_2 is not allowed, as a consequence of the above mentioned spin selection rule.

Compared to other transition metals, the oxide of Ru is particularly stable. We will discuss this case in some detail and then address the differences that occur at other metals. Interestingly, catalysis at Ru metals happens under (T, p) conditions where the bulk oxide is stable. This is not very informative about the surface composition and structure. Figure 21 A shows the surface structure that is predicted by DFT calculations under low pressure and which is indeed found in a UHV by STM.[22,142] In contrast to other rutile-structured metal oxides, the surface is practically perfect, that is, there are practically no vacancies or other defects in the O-bridge rows and no adatoms at the Ru coordinatively unsatured sites (cus). This situation is drastically changed when we look at the surface at the steady state of catalysis and under high TOF conditions. The surface is still related to RuO_2 (110), but now only about 90% of the bridge sites are occupied by O, and the Ru^{cus} atom sites are no longer

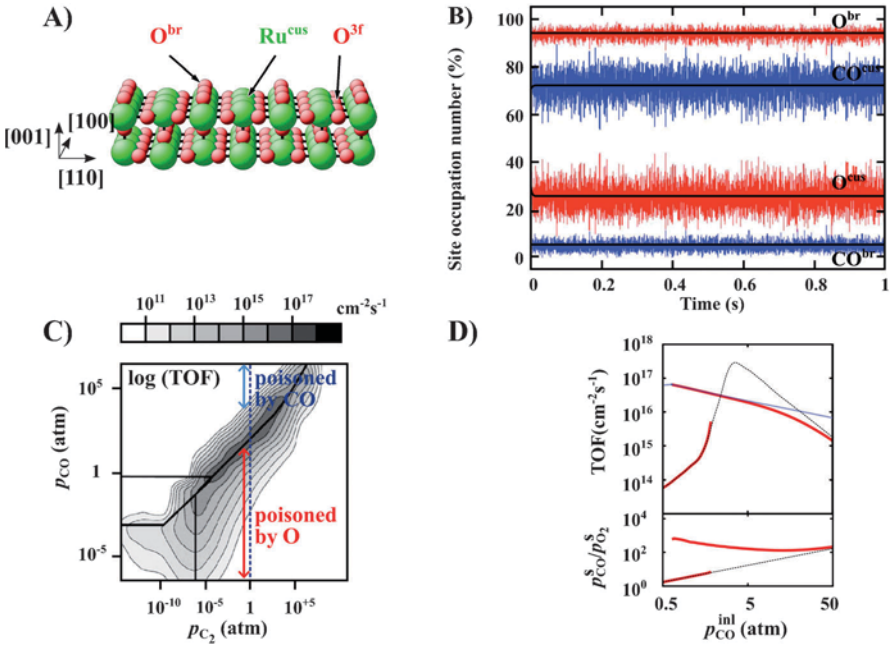

Figure 21. A) Surface structure of RuO_2 (110) under UHV conditions as predicted by DFT calculations and observed experimentally. If we ignore relaxations, this is essentially a truncated bulk geometry. The bridge sites (occupied by O^{br}), the naked Ru^{cus} atoms (cus = coordinatively unsaturated site), and the second layer threefold (3f) coordinated O^{3f} atoms are labeled. B) Time evolution of the occupation of the two prominent adsorption sites, bridge and cus, by O atoms and CO molecules. The assumed temperature and pressure conditions ($T = 600$ K, $p_{CO} = 7$ atm, $p_{O_2} = 1$ atm) correspond to the optimum catalytic performance. Under these conditions a kinetic steady-state surface population is built up in which O and CO compete for both types of sites at the surface. The fluctuations in the site occupations within the (20×20) simulation cell are significant. Note the time range for the "induction period" until the steady-state populations are reached when starting from a fully oxygen-covered surface. C) Map of calculated TOFs at $T = 600$ K. The plot is based on 400 kMC simulations for different (p_{CO}, p_{O_2}) conditions. D) Comparison of intrinsic TOFs (blue dotted line, see text) with observable TOFs (red solid line) for the CO oxidation at RuO_2(110) in a stagnation flow reactor. At the high TOFs reached at the nominal inlet temperature of 600 K, the observable TOF is for most pressures very close to the upper limit set by mass transfer through the boundary layer of products above the surface (blue line). This limit is a reactor property, independent of the employed catalyst. (From Ref. [25].)

unoccupied but occupied by CO molecules (70%) and by O adatoms (30%; see Figure 21 B).

The detailed movies of the atomic structure as a function of time that led to Figure 21 B (see Ref. [164]), together with a "sensitivity analysis",[166] reveal the importance of kinetics for understanding the high-performance conditions of catalysis: The adsorption of O_2 (dissociative) and that of CO (non-dissociative) compete for adsorption sites at the surface, specifically the bridge and the cus sites (see Figure 21 A). Here an important correlation occurs, because O_2 needs two nearby sites, while CO is happy with just one. Thus, after a catalytic reaction ($O^{ad} + CO^{ad} \rightarrow CO_2$) has happened, two empty sites remain. These can be occupied by two O adatoms (from dissociated O_2) or by CO. As soon as one CO molecule has been adsorbed, the remaining empty site is no longer sufficient for O_2 dissociation but can only accept another CO molecule. As a consequence, kinetically controlled nonrandom structures are formed,[165,166] which disable some potentially very active reaction pathways. In fact, the whole surface may get CO rich and catalytically inactive. If, and only if, the pressure is chosen properly, can adsorbed CO also desorb at a sufficiently high rate to self-heal such "poisoned" regions. Alternatively, the surface may get oxygen rich and will only get healed when some desorption of oxygen can also happen and/or chemical reactions heal these regions from their boundaries. The calculated TOF diagram as a function of O_2 and CO pressures is shown in Figure 21 C). Also indicated is that the steady state changes from an "O poisoned" surface composition to a "CO poisoned" surface composition. The optimum (high-performance) situation is found in between. In this active regime the surface (locally) proceeds from an oxygen-rich or a CO-rich to a catalytically highly active structure and back to the "bad" CO- or O-rich compositions. This change between different (local) surface structures and the accompanied activation, poisoning, and healing is what we call system chemistry, and the reason for the fluctuations visible in Figure 21 B. It reflects a specific structural instability necessary for a sustained good catalytic performance.

We mention in passing that the pressure range shown in Figure 21 C is unrealistically large, as the calculations assumed that the underlying RuO_2 material will not change its structure, except at the outermost surface region. Clearly, this is not the case in reality, as the substrate will transform to Ru metal when the CO pressure is high (compare Figure 20).

For transition metals to the right of Ru in the Periodic Table, calculations indicate that catalysis is controlled by qualitatively similar processes as discussed above. However, differences exist, as in these cases the bulk oxide is not a stable material at catalytically relevant conditions. Nevertheless, in the steady state of operation and as a result of the competition of O_2 and CO adsorption, surface oxides still play a significant role. This will now be exemplified for CO oxidation at palladium.

Figure 22 A shows the calculated phase diagram of Pd in an O_2 atmosphere as a function of temperature and pressure. As a general result, and also valid for other transition metals, we see that a surface oxide is formed well before the transition towards the bulk oxide takes place.[20,167,168] In fact, these studies also revealed that formation of the surface

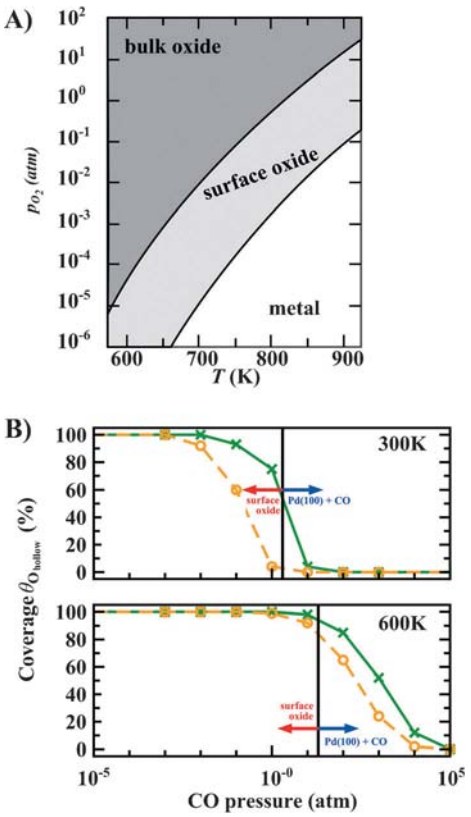

Figure 22. A) The calculated stability range of Pd bulk metal, surface oxides at Pd(100), and PdO bulk oxide at various T and p (Refs. [167,168]). B) Average occupation of hollow sites by oxygen versus CO pressure for $T = 300$ K and $T = 600$ K (from Ref. [169]). The vertical black line marks the boundary between the surface oxide and a CO-covered Pd(100) surface as determined within the constrained thermodynamics approach. The influence of the barrier on the $O^{hollow} + CO^{bridge} \rightarrow CO_2$ reaction is illustrated by showing the kMC simulation results for two barrier values of 0.9 eV (green) and 0.8 eV (orange), see text.

oxide starts after adsorption of oxygen and as soon as oxygen starts occupying subsurface sites.[168]

Under catalytic conditions, namely, when catalytic surface reactions are ongoing, the surface of Pd(100) may change, and this is reflected by the results shown in Figure 22 B. The shown simulations were performed at two different temperatures, $T = 300$ and 600 K. A noticeable limitation of this study was that the lattice was fixed to the Pd(100) structure. Thus, not all the possible surface oxides were allowed to form, which implies that surface oxides may play an even bigger role than is suggested by the shown results. For each temperature, the oxygen pressure is set to $p_{O_2} = 1$ atm, and the simulations are run at different CO pressures in the range $p_{CO} = 10^{-5}$–10^{5} atm, which covers all the possibly relevant gas-phase conditions. The graphs show a plot of the average occupation of hollow sites with oxygen at the steady state.

To get an estimate for uncertainties in the results Figure 22 B also includes results for simulations using a 0.1 eV lower barrier for the catalytic reaction $O^{hollow} + CO^{bridge} \rightarrow CO_2$, while all the other barriers were left unchanged: The DFT calculations give a reaction barrier of 0.9 eV (green

curves in Figure 22 B) and the modified barrier is 0.8 eV (orange curves). The top graph in Figure 22 B, that is, the simulations at 300 K, show that the surface oxide is stable for CO pressures up to $p_{CO} \approx 10^{-1}$ atm, that is, where 95 % of the hollow sites are occupied by O atoms. If the CO pressure is further increased, the O population at hollow sites decreases and, for CO pressures of $p_{CO} \approx 1$ atm, the surface oxide is certainly destabilized. Thus, the kinetic Monte Carlo (kMC) simulations predict that at a temperature of $T = 300$ K, oxygen-rich conditions with $p_{CO}/p_{O_2} \approx 1{:}10$ are needed to stabilize the surface oxide structure. The lower panel of Figure 22 B shows how the above picture is changed when the temperature is increased. For example, the simulation results for the highest considered temperature of $T = 600$ K reveal that the surface oxide is now actually stable up to rather sizable CO pressures. Comparing the critical p_{CO}/p_{O_2} ratio determined for the decomposition onset in the temperature range $T = 300$–600 K, the work by Rogal et al.[169] clearly identify an increasing stability of the surface oxide with increasing temperature, which, at the highest temperatures studied, reaches well up to the catalytically most relevant feeds. Furthermore, the authors found that with these feeds, the simulated turnover frequencies for the intact surface oxide alone are already of a similar order of magnitude as those reported by Szanyi and Goodman[170] for the Pd(100) surface under comparable gas-phase conditions. While a quantitative comparison is outside the scope of this discussion (and outside the accuracy of present DFT functionals), we note that, contrary to the prevalent general preconception, this particular surface oxide is clearly not "inactive" with respect to the oxidation of CO.

Let us finally address one other important aspect that has already been mentioned in the introduction, which implies that the high TOFs of Figure 21 C cannot be reached in realistic chemical reactors. The reason for this limitation is the heat and mass transport, specifically in the gas phase of a realistic reactor. To consider these aspects in quantitative multiscale modeling, the hitherto discussed first-principles statistical mechanics results (Figure 21 B,C) need to be integrated into a fluid dynamics treatment of the macroscale flow structures in the reactor. This has recently been presented by Matera and Reuter for the oxidation of CO at $RuO_2(110)$.[25] The results in Figure 21 D show representative gas-phase and flow conditions for modern in situ experiments. The blue dotted line in the upper part corresponds to the TOF of Figure 21 C. This is called "intrinsic TOF". Figure 21 D reveals the influence of the heat- and mass-transport limitations, that is, the difference between the red lines (the extrinsic TOF) and the blue lines (intrinsic TOF). Furthermore, we see that for a range of gas-phase conditions the system exhibits two stationary operation modes, a low-activity branch corresponding to the intrinsic reactivity and a high-activity branch which arises from the coupling of the surface chemistry to the surrounding flow field. Clearly, such reactor-dependent effects need to be disentangled, understood, and controlled when aiming to compare data obtained by different experimental setups, and when aiming to draw conclusions on the actual surface chemistry under technologically relevant gas-phase conditions. We note that the CO oxidation reaction is more prone to such transport effects than other more complex catalytic reactions, because the intrinsic reaction probability of this unselective reaction is very high.

7. Conclusions and Outlook

CO oxidation, although seemingly a simple chemical reaction, provides us with a panacea that reveals the richness and beauty of heterogeneous catalysis. The Fritz Haber Institut (called the "Fritz" worldwide) is a place where a multidisciplinary approach to study the course of such a heterogeneous reaction can be generated in house. Research at the institute is primarily curiosity driven, which is reflected in the five sections comprising this Review. We use an approach based on microscopic concepts to study the interaction of simple molecules with well-defined materials, such as clusters in the gas phase or solid surfaces. This approach often asks for the development of new methods, tools and materials to prove them, and it is exactly this aspect, both, with respect to experiment and theory, that is a trade mark of our institute. This enables us to develop a methodologically sound and broadly based approach.

A rather clear picture about the course of the CO oxidation reaction can be obtained by investigating a broad range of catalysts and a range of different approaches. The ability to use model systems to nanostructure materials from individual molecular clusters so as to generate stable facets under reaction conditions have allowed us to reveal the strong influence of the local structure of the binding site on chemical properties. This is demonstrated for isolated gas-phase clusters, where a rigorous identification of the geometric and electronic properties can be gained by comparison between experiment and theory. The charge state of the adsorbate–substrate complex as well as charge-transfer processes are crucial both for the understanding of chemical interaction, and also for the activation of the reaction, for example, through electronic non-adiabatic contributions. Reaction dynamics in extended systems is controlled by competing adsorbate phases limiting the free space required for sustained heterogeneous reactions. For example, complex chemical dynamics were reveled for systems where bulk and surface properties are coupled. Those range from complete coexistence of phases through patches to subsurface structures and ending at layers of support material on top of the active metal.

It is now possible to extend the strategy of the fundamental single-crystal approach pioneered by G. Ertl and G. Somorjai almost 40 years ago. As we deal with increasing complexity we are forced to relax some of the boundary conditions used in previous studies. For example, we are now in the position to go beyond studies of perfectly flat and periodic surfaces with homogeneous reaction sites and to study both local and extended electronic structures as well as reaction dynamics on various length and time scales. We can relax the strict separation between surface and bulk and allow the subsurface regime to couple to surface reactions and become more "realistic". This becomes increasingly important in the description of catalytic reactions at finite temper-

atures and pressures both theoretically and experimentally through in situ studies. Synthesizing model and high-performance catalysts with increasing control of their properties is another approach to improve the understanding of heterogeneous reactions. However, under high-performance conditions we are not only dealing with surface reactivity, we are facing challenges of transport phenomena being possibly responsible for the observed performance below the thermodynamic limits.

With the improved theoretical and experimental possibilities in hand, a detailed understanding of heterogeneous reactions may become feasible, thus leading to realistic models and providing insights into the chemical complexity of coupled gas-surface reactions with increasing precision. This has still to be extended beyond the prototype example of CO oxidation to a full reaction scheme, such as the one shown in Figure 1. These reactions are not only of key relevance for our conceptual understanding of chemical reactions but also bear considerable practical value in the emerging context of energy-storage applications. For this purpose, the simplest and most effective reactions are needed that allow effective pathways for converting energy in chemical bonds and its reversal. For this goal it is of paramount importance to understand heterogeneous reactions at the level indicated here for this prototype example of CO oxidation.

H.J.F. acknowledges crucial intellectual contributions from Thomas Risse, Niklas Nilius, Martin Sterrer, Shamil Shaikhutdinov, Markus Heyde, Helmut Kuhlenbeck, Thomas Schmidt, and Swetlana Schauermann as well as financial support from the German Science Foundation (DFG) and the Fonds der Chemischen Industrie. G.M. acknowledges detailed discussions with Andre Fielicke. M.S. acknowledges helpful, intellectual contributions from Karsten Reuter, Sergey Levchenko, and Luca Ghiringhelli, as well as financial support from UniCat, a Cluster of Excellence of the German Science Foundation (DFG). R.S. acknowledges the dedicated efforts and intellectual input from Malte Behrens, Axel Knop-Gericke, Dansheng Su, Annette Trunschke, and their teams, as well as financial support from the German Science Foundation. Multiple collaborations with the Technical University Berlin and with the Humboldt University Berlin through SFB 546 and COE UniCat contributed to the concept of this work. M.W. would like to thank Christian Frischkorn for important contributions and helpful discussions and acknowledges financial support by the German Science Foundation through SFB 450.

Received: February 24, 2011
Published online: September 29, 2011

[1] H. S. Taylor, *J. Phys. Chem.* **1926**, *30*, 145.
[2] A. B. Ray, F. O. Anderegg, *J. Am. Chem. Soc.* **1921**, *43*, 967.
[3] T. S. Kim, J. Gong, R. A. Ojifinni, *J. Am. Chem. Soc.* **2006**, *128*, 6282.
[4] a) T. Engel, G. Ertl, *J. Chem. Phys.* **1978**, *69*, 1267; b) T. Engel, G. Ertl, *Adv. Catal.* **1978**, *69*, 1267; c) T. Engel, G. Ertl in *The Chemical Physics of Solid Surfaces and heterogeneous Catalysis, Vol. 4* (Eds.: D. A. King, J. P. Woodruff), Elsevier, Amsterdam, **1982**.
[5] S. Akhter, J. M. White, *Surf. Sci.* **1986**, *171*, 527.
[6] J. Libuda, I. Meusel, J. Hoffmann, J. Hartmann, L. Piccolo, C. R. Henry, H. J. Freund, *J. Chem. Phys.* **2001**, *114*, 4669.
[7] H. J. Freund, R. P. Messmer, *Surf. Sci.* **1986**, *172*, 1.
[8] D. T. Lynch, S. E. Wanke, *J. Catal.* **1984**, *88*, 333.
[9] R. Imbihl, M. P. Cox, G. Ertl, *J. Chem. Phys.* **1985**, *83*, 1578.
[10] a) M. P. Cox, G. Ertl, R. Imbihl, *Phys. Rev. Lett.* **1985**, *54*, 1725; b) G. Ertl, *Science* **1991**, *254*, 1750.
[11] S. Jakubith, H. H. Rotermund, W. Engel, A. Vonoertzen, G. Ertl, *Phys. Rev. Lett.* **1990**, *65*, 3013.
[12] a) R. Imbihl, G. Ertl, *Chem. Rev.* **1995**, *95*, 697; b) R. Imbihl, *Surf. Sci.* **2009**, *603*, 1671.
[13] H. A. Gasteiger, N. Markovic, P. N. Ross, E. J. Cairns, *J. Phys. Chem.* **1994**, *98*, 617.
[14] T. J. Schmidt, H. A. Gasteiger, G. D. Stab, P. M. Urban, D. M. Kolb, R. J. Behm, *J. Electrochem. Soc.* **1998**, *145*, 2354.
[15] a) M. Haruta, *Catal. Today* **1997**, *36*, 153 – 166; b) M. Valden, X. Lai, D. W. Goodman, *Science* **1998**, *281*, 1647.
[16] a) G. J. Hutchings, *Catal. Today* **2005**, *100*, 55; b) A. S. K. Hashmi, G. J. Hutchings, *Angew. Chem.* **2006**, *118*, 8064; *Angew. Chem. Int. Ed.* **2006**, *45*, 7896.
[17] J. A. Rodriguez, D. W. Goodman, *Surf. Sci. Rep.* **1991**, *14*, 1.
[18] F. Gao, D. W. Goodman, *Langmuir* **2010**, *26*, 16540.
[19] Y. D. Kim, H. Over, G. Krabbes, G. Ertl, *Top. Catal.* **2001**, *14*, 95.
[20] K. Reuter, C. Stampfl, M. V. Ganduglia-Pirovano, M. Scheffler, *Chem. Phys. Lett.* **2002**, *352*, 311.
[21] D. W. Goodman, *Surf. Sci.* **1994**, *299*, 837 – 848.
[22] R. Blume, M. Hävecker, S. Zafeiratos, D. Teschner, E. Kleimenov, A. Knop-Gericke, R. Schlögl, A. Barinov, P. Dudin, M. Kiskinova, *J. Catal.* **2006**, *239*, 354.
[23] R. Schlögl, *ChemSusChem* **2010**, *3*, 209.
[24] a) D. Rosenthal, F. Girgsdies, O. Timpe, R. Blume, G. Weinberg, D. Teschner, R. Schlögl, *Z. Phys. Chem.* **2009**, *233*, 183; b) W. B. Kim, G. J. Rodriguez-Rivera, S. T. Evans, T. Voitl, J. J. Einspahr, P. M. Voyles, J. A. Dumesic, *J. Catal.* **2005**, *235*, 327; c) P. M. Couwenberg, Q. Chen, G. B. Marin, *Ind. Eng. Chem. Res.* **1996**, *35*, 3999.
[25] S. Matera, K. Reuter, *Phys. Rev. B* **2010**, *82*, 085446.
[26] P. Stoltze, J. K. Norskov, *Phys. Rev. Lett.* **1985**, *55*, 2502.
[27] G. Ertl, *Reactions at Solid Surfaces*, Wiley-VCH, Weinheim, **2009**.
[28] J. Rogal, K. Reuter, M. Scheffler, *Phys. Rev. B* **2007**, *75*, 205433.
[29] K. Reuter, M. Scheffler, *Phys. Rev. B* **2006**, *73*, 045433.
[30] G. A. Somorjai, R. M. Rioux, *Catal. Today* **2005**, *100*, 201 – 215.
[31] Y. Suchorski, C. Spiel, D. Vogel, W. Drachsel, R. Schlögl, G. Rupprechter, *ChemPhysChem* **2010**, *11*, 3231.
[32] G. Ertl, *Angew. Chem.* **2008**, *120*, 3578; *Angew. Chem. Int. Ed.* **2008**, *47*, 3524.
[33] S. Nettesheim, A. von Oertzen, H. H. Rotermund, G. Ertl, *J. Chem. Phys.* **1993**, *98*, 9977.
[34] H. Over, Y. D. Kim, A. P. Seitsonen, S. Wendt, E. Lundgren, M. Schmid, P. Varga, A. Morgante, G. Ertl, *Science* **2000**, *287*, 1474.
[35] H. S. Taylor, *Proc. R. Soc. London Ser. A* **1925**, *108*, 105.
[36] R. Schlögl, S. B. A. Hamid, *Angew. Chem.* **2004**, *116*, 1656; *Angew. Chem. Int. Ed.* **2004**, *43*, 1628.
[37] R. Meyer, C. Lemire, S. K. Shaikhutdinov, H.-J. Freund, *Gold Bull.* **2004**, *37*, 72.
[38] T. Hayashi, K. Tanaka, M. Haruta, *J. Catal.* **1998**, *178*, 566.
[39] K. R. Asmis, A. Fielicke, G. von Helden, G. Meijer in *Atomic Clusters: From Gas Phase to Deposited* (Ed.: D. P. Woodruff), Elsevier, Amsterdam, **2007**, p. 327.
[40] D. Oepts, A. F. G. van der Meer, P. W. van Amersfoort, *Infrared Phys. Technol.* **1995**, *36*, 297.

[41] A. Fielicke, G. von Helden, G. Meijer, *Eur. Phys. J. D* **2005**, *34*, 83.

[42] R. Gehrke, P. Gruene, A. Fielicke, G. Meijer, K. Reuter, *J. Chem. Phys.* **2009**, *130*, 034306.

[43] a) A. Fielicke, A. Kirilyuk, C. Ratsch, J. Behler, M. Scheffler, G. von Helden, G. Meijer, *Phys. Rev. Lett.* **2004**, *93*, 023401; b) C. Ratsch, A. Fielicke, A. Kirilyuk, J. Behler, G. von Helden, G. Meijer, M. Scheffler, *J. Chem. Phys.* **2005**, *122*, 124302; c) P. Gruene, A. Fielicke, G. Meijer, *J. Chem. Phys.* **2007**, *127*, 234307; d) A. Fielicke, P. Gruene, M. Haertelt, D. J. Harding, G. Meijer, *J. Phys. Chem. A* **2010**, *114*, 9755.

[44] A. Fielicke, C. Ratsch, G. von Helden, G. Meijer, *J. Chem. Phys.* **2007**, *127*, 234306.

[45] D. J. Harding, T. R. Walsh, S. M. Hamilton, W. S. Hopkins, S. R. Mackenzie, P. Gruene, M. Haertelt, G. Meijer, A. Fielicke, *J. Chem. Phys.* **2010**, *132*, 011101.

[46] D. J. Harding, P. Gruene, M. Haertelt, G. Meijer, A. Fielicke, S. M. Hamilton, W. S. Hopkins, S. R. Mackenzie, S. Neville, T. R. Walsh, *J. Chem. Phys.* **2010**, *133*, 214304.

[47] A. Fielicke, I. Rabin, G. Meijer, *J. Phys. Chem. A* **2006**, *110*, 8060.

[48] P. Gruene, D. M. Rayner, B. Redlich, A. F. G. van der Meer, J. T. Lyon, G. Meijer, A. Fielicke, *Science* **2008**, *321*, 674.

[49] A. Fielicke, C. Ratsch, G. von Helden, G. Meijer, *J. Chem. Phys.* **2005**, *122*, 091105.

[50] Y.-C. Bae, V. Kumar, H. Osanai, Y. Kawazoe, *Phys. Rev. B* **2005**, *72*, 125427.

[51] L. L. Wang, D. D. Johnson, *J. Phys. Chem. B* **2005**, *109*, 23113.

[52] Y. Sun, M. Zhang, R. Fournier, *Phys. Rev. B* **2008**, *77*, 075435.

[53] J. P. Perdew, K. Burke, M. Ernzerhof, *Phys. Rev. Lett.* **1996**, *77*, 3865.

[54] J. P. Perdew, M. Ernzerhof, K. Burke, *J. Chem. Phys.* **1996**, *105*, 9982.

[55] M. P. Johansson, A. Lechtken, D. Schooss, M. M. Kappes, F. Furche, *Phys. Rev. A* **2008**, *77*, 053202.

[56] F. Furche, R. Ahlrichs, P. Weis, C. Jacob, S. Gilb, T. Bierweiler, M. M. Kappes, *J. Chem. Phys.* **2002**, *117*, 6982.

[57] S. Gilb, P. Weis, F. Furche, R. Ahlrichs, M. M. Kappes, *J. Chem. Phys.* **2002**, *116*, 4094.

[58] A. Lechtken, C. Neiss, M. M. Kappes, D. Schooss, *Phys. Chem. Chem. Phys.* **2009**, *11*, 4344.

[59] X. Xing, B. Yoon, U. Landman, J. H. Parks, *Phys. Rev. B* **2006**, *74*, 165423.

[60] J. Li, X. Li, H.-J. Zhai, L.-S. Wang, *Science* **2003**, *299*, 864.

[61] S. Bulusu, X. Li, L.-S. Wang, X. C. Zeng, *Proc. Natl. Acad. Sci. USA* **2006**, *103*, 8326.

[62] D. Schooss, P. Weis, O. Hampe, M. M. Kappes, *Philos. Trans. R. Soc. London Ser. A* **2010**, *368*, 1211.

[63] L. M. Ghiringhelli, P. Gruene, J. T. Lyon, A. Fielicke, G. Meijer, M. Scheffler, unpublished results.

[64] L. M. Ghiringhelli, E. C. Beret, P. Gruene, J. T. Lyon, A. Fielicke, G. Meijer, M. Scheffler, unpublished results.

[65] Y. Shi, K. M. Ervin, *J. Chem. Phys.* **1998**, *108*, 1757–1760.

[66] L. D. Socaciu, J. Hagen, T. M. Bernhardt, L. Wöste, U. Heiz, H. Häkkinen, U. Landman, *J. Am. Chem. Soc.* **2003**, *125*, 10437.

[67] A. Fielicke, P. Gruene, G. Meijer, D. M. Rayner, *Surf. Sci.* **2009**, *603*, 1427.

[68] G. Brodén, T. N. Rhodin, C. Brucker, R. Benbow, Z. Hurych, *Surf. Sci.* **1976**, *59*, 593.

[69] J. T. Lyon, P. Gruene, A. Fielicke, G. Meijer, D. M. Rayner, *J. Chem. Phys.* **2009**, *131*, 184706.

[70] S. S. Sung, R. Hoffmann, *J. Am. Chem. Soc.* **1985**, *107*, 578.

[71] M. Gajdos, A. Eichler, J. Hafner, *J. Phys. Condens. Matter* **2004**, *16*, 1141.

[72] B. Hammer, J. K. Norskov, *Adv. Catal.* **2000**, *45*, 71.

[73] N. Sheppard, T. T. Nguyen in *Advances in Infrared and Raman Spectroscopy*, *Vol. 5* (Eds.: R. E. Hester, R. J. H. Clark), Heyden, London, **1978**, p. 67.

[74] G. Blyholder, *J. Phys. Chem.* **1964**, *68*, 2772.

[75] A. Fielicke, G. von Helden, G. Meijer, D. B. Pedersen, B. Simard, D. M. Rayner, *J. Phys. Chem. B* **2004**, *108*, 14591.

[76] P. Gruene, A. Fielicke, G. Meijer, D. M. Rayner, *Phys. Chem. Chem. Phys.* **2008**, *10*, 6144.

[77] A. Fielicke, G. von Helden, G. Meijer, D. B. Pedersen, B. Simard, D. M. Rayner, *J. Chem. Phys.* **2006**, *124*, 194305.

[78] M. Frank, M. Bäumer, R. Kühnemuth, H.-J. Freund, *J. Phys. Chem. B* **2001**, *105*, 8569.

[79] M. Sterrer, M. Yulikov, T. Risse, H.-J. Freund, J. Carrasco, F. Illas, C. D. Valentin, L. Giordano, G. Pacchioni, *Angew. Chem.* **2006**, *118*, 2695; *Angew. Chem. Int. Ed.* **2006**, *45*, 2633.

[80] A. Fielicke, G. von Helden, G. Meijer, B. Simard, D. M. Rayner, *J. Chem. Phys. B* **2005**, *109*, 23935.

[81] I. Swart, F. M. F. de Groot, B. M. Weckhuysen, P. Gruene, G. Meijer, A. Fielicke, *J. Phys. Chem. A* **2008**, *112*, 1139.

[82] I. Swart, A. Fielicke, B, Redlich, G. Meijer, B. M. Weckhuysen, F. M. F. de Groot, *J. Am. Chem. Soc.* **2007**, *129*, 2516.

[83] I. Swart, A. Fielicke, D. M. Rayner, G. Meijer, B. M. Weckhuysen, F. M. F. de Groot, *Angew. Chem.* **2007**, *119*, 5411; *Angew. Chem. Int. Ed.* **2007**, *46*, 5317.

[84] E. C. Beret, L. M. Ghiringhelli, M. Scheffler, unpublished results.

[85] M. G. Evans, M. Polanyi, *Trans. Faraday Soc.* **1935**, *31*, 875.

[86] G. A. Worth, L. S. Cederbaum, *Annu. Rev. Phys. Chem.* **2004**, *55*, 127.

[87] A. M. Wodtke, J. C. Tully, D. J. Auerbach, *Int. Rev. Phys. Chem.* **2004**, *23*, 513.

[88] T. Greber, *Surf. Sci. Rep.* **1997**, *28*, 3.

[89] H. Nienhaus, *Surf. Sci. Rep.* **2002**, *45*, 3.

[90] F. Budde, T. F. Heinz, M. M. T. Loy, J. A. Misewich, F. Derougemont, H. Zacharias, *Phys. Rev. Lett.* **1991**, *66*, 3024.

[91] C. Frischkorn, M. Wolf, *Chem. Rev.* **2006**, *106*, 4207.

[92] M. Brandbyge, P. Hedegard, T. F. Heinz, J. A. Misewich, D. M. Newns, *Phys. Rev. B* **1995**, *52*, 6042.

[93] M. Lisowski, P. A. Loukakos, U. Bovensiepen, J. A. Stähler, C. Gahl, M. Wolf, *Appl. Phys. A* **2004**, *78*, 165.

[94] F. Schmitt, P. Kirchmann, U. Bovensiepen, R. G. Moore, L. Rettig, M. Krenz, J.-H. Chu, N. Ru, L. Perfetti, D. H. Lu, M. Wolf, I. Fisher, Z.-X. Shen, *Science* **2008**, *321*, 1649.

[95] M. Bonn, C. Hess, S. Funk, J. H. Miners, B. N. J. Persson, M. Wolf, G. Ertl, *Phys. Rev. Lett.* **2000**, *84*, 4653.

[96] M. Bonn, S. Funk, C. Hess, D. N. Denzler, C. Stampfl, M. Scheffler, M. Wolf, G. Ertl, *Science* **1999**, *285*, 1042.

[97] J. A. Prybyla, T. F. Heinz, J. A. Misewich, M. M. Loy, J. H. Glownia, *Phys. Rev. Lett.* **1990**, *64*, 1537.

[98] S. Funk, M. Bonn, D. N. Denzler, Ch. Hess, M. Wolf, G. Ertl, *J. Chem. Phys.* **2000**, *112*, 9888.

[99] C. Stampfl, M. Scheffler, *Phys. Rev. B* **2008**, *54*, 2868.

[100] a) D. N. Denzler, C. Frischkorn, C. Hess, M. Wolf, G. Ertl, *Phys. Rev. Lett.* **2003**, *91*, 226102; b) D. N. Denzler, C. Frischkorn, C. Hess, M. Wolf, G. Ertl, *J. Phys. Chem. B* **2004**, *108*, 14503.

[101] a) S. Wagner, C. Frischkorn, M. Wolf, M. Rutkowski, H. Zacharias, A. C. Luntz, *Phys. Rev. B* **2005**, *72*, 205404; b) A. C. Luntz, M. Persson, S. Wagner, C. Frischkorn, M. Wolf, *J. Chem. Phys.* **2006**, *124*, 244702.

[102] G. Ertl, H. Knözinger, F. Schüth, J. Weitkamp, *Handbook of Heterogeneous Catalysis*, *Vol. 4*, Wiley-VCH, Weinheim, **2008**.

[103] G. Ertl, H.-J. Freund, *Phys. Today* **1999**, *52*, 32.

[104] a) H.-J. Freund, *Angew. Chem.* **1997**, *109*, 444; *Angew. Chem. Int. Ed. Engl.* **1997**, *36*, 452; b) H.-J. Freund, *Surf. Sci.* **2002**, *500*, 271; c) H.-J. Freund, H. Kuhlenbeck, V. Staemmler, *Rep. Prog. Phys.* **1996**, *59*, 283.

[105] H.-J. Freund, D. W. Goodman in *Handbook of Heterogeneous Catalysis* (Eds.: G. Ertl, H. Knözinger, F. Schüth, J. Weitkamp), Wiley-VCH, Weinheim, **2007**.

[106] M. Haruta, *Cattech* **2002**, *6*, 102.

[107] T. Risse, S. Shaikhutdinov, N. Nilius, M. Sterrer, H.-J. Freund, *Acc. Chem. Res.* **2008**, *41*, 949.

[108] G. J. Hutchings, M. Brust, H. Schmidbaur, *Chem. Soc. Rev.* **2008**, *37*, 1759.

[109] a) M. Yulikov, M. Sterrer, M. Heyde, H. P. Rust, T. Risse, H.-J. Freund, G. Pacchioni, A. Scagnelli, *Phys. Rev. Lett.* **2006**, *96*, 146804; b) M. Sterrer, M. Yulikov, E. Fischbach, M. Heyde, H.-P. Rust, G. Pacchioni, T. Risse, H. J. Freund, *Angew. Chem.* **2006**, *118*, 2692; *Angew. Chem. Int. Ed.* **2006**, *45*, 2630; c) Ref. [79]; d) M. Sterrer, T. Risse, U. Martinez Pozzoni, L. Giordano, M. Heyde, H.-P. Rust, G. Pacchioni, H.-J. Freund, *Phys. Rev. Lett.* **2007**, *98*, 096107.

[110] V. Simic-Milosevic, M. Heyde, X. Lin, T. König, H.-P. Rust, M. Sterrer, T. Risse, N. Nilius, H.-J. Freund, L. Giordano, G. Pacchioni, *Phys. Rev. B* **2008**, *78*, 235429.

[111] M. Sterrer, T. Risse, M. Heyde, H.-P. Rust, H.-J. Freund, *Phys. Rev. Lett.* **2007**, *98*, 206103.

[112] C. Freysoldt, P. Rinke, M. Scheffler, *Phys. Rev. Lett.* **2007**, *99*, 086101.

[113] X. Lin, N. Nilius, H. J. Freund, M. Walter, P. Frondelius, K. Honkala, H. Häkkinen, *Phys. Rev. Lett.* **2009**, *102*, 206801.

[114] V. Simic-Milosevic, M. Heyde, N. Nilius, T. Koenig, H. P. Rust, M. Sterrer, T. Risse, H. J. Freund, L. Giordano, G. Pacchioni, *J. Am. Chem. Soc.* **2008**, *130*, 7814.

[115] J. J. Schulz, R. Koch, K. H. Rieder, *Phys. Rev. Lett.* **2000**, *84*, 4597.

[116] L. Bartels, G. Meyer, K. H. Rieder, *Phys. Rev. Lett.* **1997**, *79*, 697.

[117] N. Nilius, M. V. Ganduglia-Pirovano, V. Brázdová, M. Kulawik, J. Sauer, H. J. Freund, *Phys. Rev. Lett.* **2008**, *100*, 096802.

[118] X. Lin, N. Nilius, M. Sterrer, P. Koskinen, H. Häkkinen, H.-J. Freund, *Phys. Rev. B* **2010**, *81*, 153406.

[119] X. Lin, B. Yang, H.-M. Benia, P. Myrach, M. Yulikov, A. Aumer, M. Brown, M. Sterrer, O. Bondarchuk, E. Kieseritzky, J. Rocker, T. Risse, H. Gao, N. Nilius, H. J. Freund, *J. Am. Chem. Soc.* **2010**, *132*, 7745.

[120] F. C. M. J. M. Van Delft, B. E. Nieuwenhuys, *Solid State Ionics* **1985**, *16*, 233.

[121] A. D. Logan, E. J. Braunschweig, A. K. Datye, D. J. Smith, *Langmuir* **1988**, *4*, 827.

[122] O. Dulub, W. Hebenstreit, U. Diebold, *Phys. Rev. Lett.* **2000**, *84*, 3646.

[123] M. Bowker, *Surf. Sci.* **2009**, *603*, 2359.

[124] a) Y. N. Sun, L. Giordano, J. Goniakowski, M. Lewandowski, Z. H. Qin, C. Noguera, S. Shaikhutdinov, G. Pacchioni, H. J. Freund, *Angew. Chem.* **2010**, *122*, 4520; *Angew. Chem. Int. Ed.* **2010**, *49*, 4418; b) Y. N. Sun, Z. H. Qin, M. Lewandowski, E. Carrasco, M. Sterrer, S. Shaikhutdinov, H. J. Freund, *J. Catal.* **2009**, *266*, 359; c) Z. H. Qin, M. Lewandowski, Y. N. Sun, S. Shaikhutdinov, H. J. Freund, *J. Phys. Chem. C* **2008**, *112*, 10209.

[125] a) Z. H. Qin, M. Lewandowski, Y. N. Sun, S. Shaikhutdinov, H. J. Freund, *J. Phys. Condens. Matter* **2009**, *21*, 134019; b) M. Lewandowski, Y. N. Sun, Z. H. Qin, S. Shaikhutdinov, H. J. Freund, *Appl. Catal. A* **2011**, *391*, 407; c) Y. N. Sun, Z. H. Qin, M. Lewandowski, S. Kaya, S. Shaikhutdinov, H. J. Freund, *Catal. Lett.* **2008**, *126*, 31.

[126] K. H. Hansen, T. Worren, S. Stempel, E. Lægsgaard, M. Bäumer, H. J. Freund, F. Besenbacher, I. Stensgaard, *Phys. Rev. Lett.* **1999**, *83*, 4120.

[127] a) H. C. Galloway, J. J. Benítez, M. Salmeron, *Surf. Sci.* **1993**, *298*, 127; b) Y. J. Kim, C. Westphal, R. X. Ynzunza, H. C. Galloway, M. Salmeron, M. A. Van Hove, C. S. Fadley, *Phys. Rev. B* **1997**, *55*, R13448.

[128] a) W. Weiss, A. Barbieri, M. A. Van Hove, G. A. Somorjai, *Phys. Rev. Lett.* **1993**, *71*, 1848; b) G. H. Vurens, V. Maurice, M. Salmeron, G. A. Somorjai, *Surf. Sci.* **1992**, *268*, 170; c) G. H. Vurens, M. Salmeron, G. A. Somorjai, *Surf. Sci.* **1988**, *201*, 129.

[129] M. Ritter, W. Ranke, W. Weiss, *Phys. Rev. B* **1998**, *57*, 7240.

[130] T. Schalow, B. Brandt, D. E. Starr, M. Laurin, S. Shaikhutdinov, S. Schauermann, J. Libuda, H. J. Freund, *Angew. Chem.* **2006**, *118*, 3775; *Angew. Chem. Int. Ed.* **2006**, *45*, 3693.

[131] M. Lewandowski, PhD thesis, Technical University Berlin, **2011**, in preparation.

[132] N. Cabrera, N. F. Mott, *Rep. Prog. Phys.* **1948**, *12*, 163.

[133] F. F. Vol'kenshtein, *Russ. Chem. Rev.* **1966**, *35*, 537.

[134] J. C. Frost, *Nature* **1988**, *334*, 577.

[135] M. Boudart, *Catal. Lett.* **1992**, *13*, 153.

[136] V. Ponec, *Catal. Lett.* **1991**, *11*, 249.

[137] a) T. Kim, I. E. Wachs, *J. Catal.* **2008**, *255*, 197; b) D. Kulkarni, I. E. Wachs, *Appl. Catal. A* **2002**, *237*, 121.

[138] a) R. K. Grasselli, D. J. Buttrey, J. D. Burrington, A. Andersson, J. Holmberg, W. Ueda, J. Kubo, C. G. Lugmair, A. F. Volpe, Jr., *Top. Catal.* **2006**, *38*, 7–16; b) A. Celaya Sanfiz, T. W. Hansen, A. Sakthivel, R. Schlögl, A. Knoester, H. H. Brongersma, M. H. Looi, S. B. A. Hamid, *J. Catal.* **2008**, *258*, 35; c) A. C. Sanfiz, T. W. Hansen, D. Teschner, P. Schnorch, F. Girgsdies, A. Trunschke, R. Schlögl, M. H. Looi, S. B. A. Hamid, *J. Phys. Chem. C* **2010**, *114*, 1912.

[139] a) X. Rozanska, R. Fortrie, J. Sauer, *J. Phys. Chem. C* **2007**, *111*, 6041; b) X. Rozanska, E. V. Kondratenko, J. Sauer, *J. Catal.* **2008**, *256*, 84–94.

[140] a) A. Böttcher, H. Conrad, H. Niehus, *Surf. Sci.* **2000**, *452*, 125; b) A. Böttcher, H. Conrad, H. Niehus, *J. Chem. Phys.* **2000**, *112*, 4779.

[141] a) R. Blume, H. Niehus, H. Conrad, A. Böttcher, L. Aballe, L. Gregoratti, A. Barinov, M. Kiskinova, *J. Phys. Chem. B* **2005**, *109*, 14052; b) H. Bluhm, M. Havecker, A. Knop-Gericke, M. Kiskinova, R. Schlögl, M. Salmeron, *MRS Bull.* **2007**, *32*, 1022.

[142] Y. D. Kim, A. P. Seitsonen, S. Wendt, J. Wang, C. Fan, K. Jacobi, H. Over, G. Ertl, *J. Phys. Chem. B* **2001**, *105*, 3752.

[143] A. Böttcher, U. Starke, H. Conrad, R. Blume, H. Niehus, L. Gregoratti, B. Kaulich, A. Barinov, M. Kiskinova, *J. Chem. Phys.* **2002**, *117*, 8104.

[144] A. Knop-Gericke, E. Kleimenov, M. Havecker, R. Blume, D. Teschner, S. Zafeiratos, R. Schlögl, V. I. Bukhtiyarov, V. V. Kaichev, I. P. Prosvirin, A. I. Nizovskii, H. Bluhm, A. Barinov, P. Dudin, M. Kiskinova, *Adv. Catal.* **2009**, *52*, 213.

[145] R. Blume, M. Hävecker, S. Zafeiratos, D. Teschner, E. Vass, P. Schnörch, A. Knop-Gericke, R. Schlögl, S. Lizzit, P. Dudin, A. Barinov, M. Kiskinova, *Phys. Chem. Chem. Phys.* **2007**, *9*, 3648.

[146] J. Assmann, V. Narkhede, L. Khodeir, E. Loffler, O. Hinrichsen, A. Birkner, H. Over, M. Muhler, *J. Phys. Chem. B* **2004**, *108*, 14634.

[147] D. Rosenthal, F. Girgsdies, O. Timpe, R. Blume, G. Weinberg, D. Teschner, R. Schlögl, *Z. Phys. Chem.* **2009**, *223*, 183.

[148] Ref. [147].

[149] C. Stampfl, M. V. Ganduglia-Pirovano, K. Reuter, M. Scheffler, *Surf. Sci.* **2002**, *500*, 368.

[150] K. Reuter, M. Scheffler, *Phys. Rev. B* **2003**, *68*, 045407.

[151] Ref. [141].

[152] S. Abate, R. Arrigo, M. E. Schuster, S. Perathoner, G. Centi, A. Villa, D. Su, R. Schlogl, *Catal. Today* **2010**, *157*, 280.

[153] Y. N. Sun, Z. H. Qin, M. Lewandowski, S. Shaikhutdinov, H. J. Freund, *Surf. Sci.* **2009**, *603*, 3099–3103.

[154] J. H. Fischer-Wolfarth, J. A. Farmer, J. M. Flores-Camacho, A. Genest, I. V. Yudanov, N. Rosch, C. T. Campbell, S. Schauermann, H. J. Freund, *Phys. Rev. B* **2010**, *81*, 241416.

[155] A. Dandekar, M. A. Vannice, *J. Catal.* **1999**, *183*, 344–354.

[156] a) F. Atamny, A. Baiker, *Surf. Interface Anal.* **1999**, *27*, 512; b) P. Albers, J. Pietsch, S. F. Parker, *J. Mol. Catal. A* **2001**, *173*, 275 – 286.
[157] "Ab initio atomistic thermodynamics and statistical mechanics of surface properties and functions": K. Reuter, C. Stampfl, M. Scheffler in *Handbook of Materials Modeling*, *Vol. 1* (Ed.: S. Yip), Springer, Berlin, **2005**.
[158] J. Gustafson, R. Westerström, O. Balmes, A. Resta, R. van Rijn, X. Torrelles, C. T. Herbschleb, J. W. M. Frenken, E. Lundgren, *J. Phys. Chem. C* **2010**, *114*, 4580.
[159] M. D. Ackermann, T. M. Pedersen, B. L. M. Hendriksen, O. Robach, S. C. Bobaru, I. Popa, C. Quiros, H. Kim, B. Hammer, S. Ferrer, J. W. M. Frenken, *Phys. Rev. Lett.* **2005**, *95*, 255505.
[160] F. Tao, S. Dag, L. W. Wang, Z. Liu, D. R. Butcher, H. Bluhm, M. Salmeron, G. A. Somorjai, *Science* **2010**, *327*, 850.
[161] a) Y. Lei, F. Mehmood, S. Lee, J. Greeley, B. Lee, S. Seifert, R. E. Winans, J. W. Elam, R. J. Meyer, P. C. Redfern, D. Teschner, R. Schlogl, M. J. Pellin, L. A. Curtiss, S. Vajda, *Science* **2010**, *328*, 224; b) D. Teschner, J. Borsodi, A. Wootsch, Z. Revay, M. Havecker, A. Knop-Gericke, S. D. Jackson, R. Schlögl, *Science* **2008**, *320*, 86.
[162] G. Rupprechter, H. Unterhalt, H.-J. Freund, *Phys. Rev. Lett.* **2000**, *85*, 776.
[163] K. Reuter, M. Scheffler, *Appl. Phys. A* **2004**, *78*, 793.
[164] Movies of the site occupations that are the source of Figure 21 B are shown at http://www.fhi-berlin.mpg.de/th/movies/catalytic-CO-oxidation.
[165] R. M. Ziff, E. Gulari, Y. Barshad, *Phys. Rev. Lett.* **1986**, *56*, 2553.
[166] H. Meskine, S. Matera, M. Scheffler, K. Reuter, H. Metiu, *Surf. Sci.* **2009**, *603*, 1724.
[167] E. Lundgren, J. Gustafson, A. Mikkelsen, J. N. Andersen, A. Stierle, H. Dosch, M. Todorova, J. Rogal, K. Reuter, M. Scheffler, *Phys. Rev. Lett.* **2004**, *92*, 046101.
[168] M. Todorova, W. X. Li, M. V. Ganduglia-Pirovano, C. Stampfl, K. Reuter, M. Scheffler, *Phys. Rev. Lett.* **2002**, *89*, 096103.
[169] a) J. Rogal, K. Reuter, M. Scheffler, *Phys. Rev. Lett.* **2007**, *98*, 046101; b) J. Rogal, K. Reuter, M. Scheffler, *Phys. Rev. B* **2008**, *77*, 155410.
[170] J. Szanyi, D. W. Goodman, *J. Phys. Chem.* **1994**, *98*, 2972.